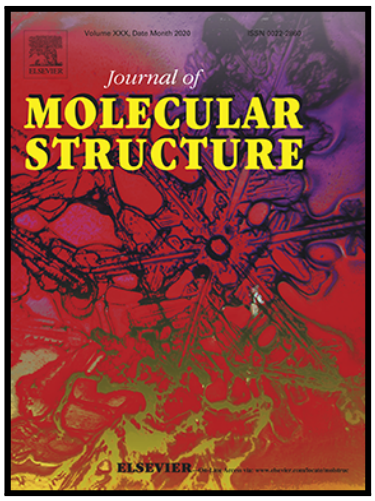

Structural characterization, DFT calculations, ADMET studies, antibiotic potentiating activity, evaluation of efflux pump inhibition and molecular docking of chalcone (E)-1-(2-hydroxy-3,4,6-trimethoxyphenyl)-3-(4-methoxyphenyl)prop-2-en-1-one

Jayze da Cunha Xavier Investigation. Data curation. Formal analysis , Francisco Wagner Queiroz Almeida-Neto , Priscila Teixeira da Silva , Amanda Pereira de Sousa , Emmanuel Silva Marinho , Márcia Machado Marinho , Janaina Esmeraldo Rocha , Priscila Ramos Freitas , Ana Carolina Justino de Araújo , Thiago Santiago Freitas , Carlos Emídio Sampaio Nogueira , Pedro de Lima-Neto , Paulo Nogueira Bandeira , Alexandre Magno Rodrigues Teixeira , Henrique Douglas Melo Coutinho , Hélcio Silva dos Santos

PII: S0022-2860(20)32005-6
DOI: https://doi.org/10.1016/j.molstruc.2020.129692
Reference: MOLSTR 129692

To appear in: *Journal of Molecular Structure*

Received date: 2 August 2020
Revised date: 12 November 2020
Accepted date: 26 November 2020

Please cite this article as: Jayze da Cunha Xavier Investigation. Data curation. Formal analysis , Francisco Wagner Queiroz Almeida-Neto , Priscila Teixeira da Silva , Amanda Pereira de Sousa , Emmanuel Silva Marinho , Márcia Machado Marinho , Janaina Esmeraldo Rocha , Priscila Ramos Freitas , Ana Carolina Justino de Araújo , Thiago Santiago Freitas , Carlos Emídio Sampaio Nogueira , Pedro de Lima-Neto , Paulo Nogueira Bandeira , Alexandre Magno Rodrigues Teixeira , Henrique Douglas Melo Coutinho , Hélcio Silva dos Santos , Structural characterization, DFT calculations, ADMET studies, antibiotic potentiating activity, evaluation of efflux pump inhibition and molecular docking of chalcone (E)-1-(2-hydroxy-3,4,6-trimethoxyphenyl)-3-(4-methoxyphenyl)prop-2-en-1-one, *Journal of Molecular Structure* (2020), doi: https://doi.org/10.1016/j.molstruc.2020.129692

Structural characterization, DFT calculations, ADMET studies, antibiotic potentiating activity, evaluation of efflux pump inhibition and molecular docking of chalcone (*E*)-1-(2-hydroxy-3,4,6-trimethoxyphenyl)-3-(4-methoxyphenyl)prop-2-en-1-one

Jayze da Cunha Xavier[a], Francisco Wagner Queiroz Almeida-Neto[b], Priscila Teixeira da Silva[a], Amanda Pereira de Sousa[f], Emmanuel Silva Marinho[c], Márcia Machado Marinho[g], Janaina Esmeraldo Rocha[a], Priscila Ramos Freitas, Ana Carolina Justino de Araújo[a], Thiago Santiago Freitas[a], Carlos Emídio Sampaio Nogueira[a,e], Pedro de Lima-Neto[b], Paulo Nogueira Bandeira[f], Alexandre Magno Rodrigues Teixeira[a], Henrique Douglas Melo Coutinho[a], Hélcio Silva dos Santos[a,d,f*]

[a] Department of Biological Chemistry, Regional University of Cariri, Crato, CE, Brazil,

[*]Corresponding author. Postgraduate Program in Biological Chemistry, Department of Biological Chemistry, Regional University of Cariri, Campus Pimenta II, CEP: 63.100-000, Crato, CE, Brazil. E-mail addresses: helciodossantos@gmail.com

HIGHLIGHTS

- A chalcone was synthesized by Claisen-Schmidt condensation reaction.
- Structural, electronic and reactivity properties were obtained using DFT.
- ADMET studies were made.
- Antimicrobial activities assays were done.
- Molecular docking studies were carried out.

[b]Group of Theoretical Chemistry, Department of Analytical Chemistry and Physical Chemistry, Federal University of Ceará, Fortaleza, CE, Brazil

[c]Group of Theoretical Chemistry and Electrochemistry, State University of Ceará, Campus FAFIDAM, Limoeiro do Norte, CE, Brazil.

[d]Science and Technology Center, Postgraduate Program in Natural Sciences, State University of Ceará, Fortaleza, CE, Brazil

[e]Department of Physics, Regional University of Cariri, Juazeiro do Norte, CE, Brazil.

[f]Center for Exact Sciences and Technology - Chemistry Course, Vale do Acaraú University, Sobral, CE, Brazil

[g]Iguatu Faculty of Education, Science and Letters (Fecli), State University of Ceará, Iguatu, Ceará, Brazil

Graphical abstrcats

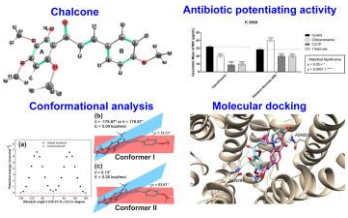

Abstract

Chalcones are open-chain flavonoids characterized by two aromatic rings joined by a three-carbon α,β-unsaturated carbonyl system. Over the last several years, chalcones have instigated the interest of chemical and pharmacological researchers due to their simple chemical structure and varied biological activities. Here, we performed the electronic properties, of the chalcone, (*E*)-1-(2-hydroxy-3,4,6-trimethoxyphenyl)-3-(4-methoxyphenyl) prop-2-en-1-one synthesized by Claisen-Schmidt condensation reaction. The density functional theory method was used with the B3LYP/6-311++G(d,p) level of theory to compute the structural, electronic, and reactivity properties of the chalcone. In addition, microbiological tests were performed to investigate the modulator potential and efflux pump inhibition on *Staphylococcus aureus* multi-resistant strains. The spectroscopic data analyses allowed drawing the molecular structure of the chalcone synthetized with subsequent confirmation using the quantum chemical calculations. The addition of chalcone to the growth medium caused a synergic effect by reduction of the minimum inhibitory concentration (MIC) values for ciprofloxacin strain. Docking results showed that the chalcone docks in almost the same way as the antibiotic against a MepA model. Druglikeness criteria based on the rules of Lipinski and Veber evaluated that the chalcone has the ideal physicochemical and pharmacokinetic properties to be a good candidate for drug orally. The results confirm the structure of the synthesized chalcone and revealing that the compound can be used as a possible inhibitor of the Mep A efflux pump.

Keywords: Chalcone, ATR-FTIR; UV-Vis; Fukui, efflux pump

1. Introduction

The search for new drugs is increasing due to the rapid growth of bacterial resistance that has become a medical concern today [1-3]. The bacterial resistance comes from factors such as selectivity (low plasma membrane permeability), adherence of the drug to the cell wall, its expulsion by efflux pumps, and the action of enzymes minimizing or inhibiting the antibiotic action [4, 5]. Among bacterial pathogens, *S. aureus,* despite being present in the skin and nasal mucosa, is capable of causing many infections and diseases both in animals and in humans since skin infections [6], toxic shock syndrome [7], to sepsis [8]. These opportunists reach debilitated people in hospitals and are difficult to treat. Fighting these infections has become a difficult problem for health worldwide due to the growth of bacterial resistance to antibiotics [9]. In this sense, there are current interests in finding new antimicrobial agents [10].

Understanding the mechanism of action and metabolism of the biologically active molecules depends, to a large extent, on the analysis of its reactivity, which is determined by intermolecular forces, that is, lipophilic, polar, electrostatic, and stereo interactions, which depend on the characteristics of each molecule (electronic, Steric or conformational, energetic and thermodynamic [11, 12]. It is precisely at this point that molecular modeling techniques can make their contribution to the study and development of active molecules because through it you can have a detailed description of the structure, intermolecular interactions, and, if applicable, chemical reactions between the ligand and biomacromolecules with chalcones [13-16].

Also, the electronic properties with respect to the frontier molecular orbitals, the quantum reactivity descriptors, the Fukui functions (electronic and condensed), and the molecular electrostatic potential were applied to characterize the reactive electrophilic and nucleophilic sites, which is extremely important because in previous studies the higher reactivity and electrophilicity of a synthetic chalcone, can be responsible for intermediated interactions with the bacterial cell wall and when combined with the gentamicin drug proved to be more efficient [17].

Previous studies showed that synthetic chalcones associated with antibiotics had obtained increasingly satisfactory results in containing resistant pathogen [18-24].

Chalcones are precursors to flavonoids and isoflavonoids [25, 26], but they can also be obtained by synthesis [23, 27]. This class of compound has aroused much interest due to the broad spectrum of pharmacological activities that they present, including antimicrobial [23, 28], antioxidant [29], antinociceptive [30, 31], antiparasitic [32], antitumor [33], and antiproliferative activities [34].

In this work, the chalcone (*E*)-1-(2-hydroxy-3,4,6-trimethoxyphenyl)-3-(4-methoxyphenyl) prop-2-en-1-one ($C_{19}H_{20}O_6$) was synthesized by Claisen-Schmidt condensation reaction. The molecular structure was characterized by spectroscopy methods, and the Density Functional Theory was used to determine the electronic and reactivity properties. In addition, microbiological tests were performed to investigate the modulator potential and efflux pump inhibition on *S. aureus* multi-resistant strains.

2. Material and methods

2.1 Spectroscopic methods: NMR, FTIR, UV-vis

The chemical reagents were purchased from Sigma-Aldrich. ^{1}H and ^{13}C NMR spectra were obtained using a Bruker Spectrometer, model Avance DPX-500, operating at a frequency of 500 MHz for hydrogen and 125 MHz for carbon, respectively. The spectra were measured in $CDCl_3$, and chemical shifts are reported as δ values in parts per million (ppm) relative to $CDCl_3$. The attenuated total reflectance Fourier transform infrared spectroscopy (ATR-FTIR) was performed using a Bruker vacuum infrared spectrometer VERTEX 70V. The measurements were recorded at room temperature in the range 400 to 4000 cm^{-1}, with a resolution of 2 cm^{-1} and accumulating 60 scans per spectrum. The UV-Visible absorption spectrum of the compound was obtained using a GENESYS 10S UV-Vis spectrophotometer (Thermo Scientific, Waltham, MA, USA) in the wavelength range of 210 to 400 nm with spectral resolution (1.8 nm). The samples were prepared at a concentration of 0.1 mmol L^{-1} using ethanol as a solvent to perform the absorption measurements in the UV-Vis region. All absorption measurements were carried out at room temperature in quartz cells with 1 cm optical path.

2.2 Synthesis of the chalcone

The compounds 2-hydroxy-3,4,6 trimethoxyacetophenone (2 mmol) and **Anisaldehyde** (2 mmol) were placed in a volumetric flask (25 mL). Then 5 mL of ethanolic NaOH (50%) solution was added and mixed with stirring for 48 h at room temperature. The progress of the reaction was checked by TLC (n-hexane: ethyl acetate, 2:1). After 48 h, the reaction mixture was neutralized with dilute HCl (10%) and ice water added. The product was obtained as a yellow solid filtered under reduced pressure, washed with cold water, and recrystallized from ethanol [27, 35] (Scheme 1).

2.3 Quantum chemical computational calculations

The quantum chemical calculations were used extensively to support the experimental data during the structural characterization of a newly synthesized molecule using the density functional theory (DFT) method. From a previous work from our group, three DFT methods were compared for the characterization of a chalcone acetamide derivative (PAAPFBA) [17], and all the methods used were accurate to describe the structural and electronic properties of a chalcone derivative molecule. Hence, due to the low computational cost, the title chalcone was geometrically optimized using the exchange-correlation functional B3LYP at the 6-311++G(d,p) basis set [36, 37], which was the same method used in other work of our group to describe the structural and electronic properties of the chalcone derivative (2*E*,4*E*)-1-(2-hydroxy-3,4,6-trimethoxyphenyl)-5-phenylpenta-2,4-dien-1-one (cinnamaldehyde) [38]. The quantum chemical calculations were carried out using the Gaussian 09 [39] software and the Gauss View 5 [40] to draw the input molecule. The optimization was done with chloroform as an implicit solvent using the IEF-PCM solvation model [41-43] available in Gaussian 09. Conformational analysis was carried from the optimized structure to obtain the potential energy surface (PES). Next, the fundamental vibrational modes were computed at the same level of theory together with the thermodynamic properties at 298.15 K and 1 atm of pressure. The absence of negative

frequencies implies that the simulated molecule can be used to describe the structural and electronic properties of the newly synthesized chalcone. The infrared spectrum was obtained from the optimized molecular geometry, and the theoretical wavenumbers were scaled by 0.983 for below 1700 cm^{-1} and by 0.958 for above 1700 cm^{-1} [44]. The theoretical assignments of the highlighted band from the experimental infrared spectrum were done using the potential energy distribution (PED) with the VEDA [45] software, and only the PED $\geq$ 10% were considered. Then, the ^{1}H and ^{13}C NMR spectra were calculated using the GIAO method [46-48] available in Gaussian 09 to obtain the theoretical isotropic shielding for the carbon (σ_C) and hydrogen (σ_H) atoms. Tetramethylsilane (TMS) was used as a reference compound to calculate the theoretical chemical shifts as follows: $\delta_C = \sigma_{C(TMS)} - \sigma_C$ and $\delta_H = \sigma_{H(TMS)} - \sigma_H$. The frontier molecular orbitals (FMO) were calculated from the optimization calculation to understand the electronic density distribution over the entire molecule and the energy values of those molecular orbitals were used to compute the global quantum reactivity descriptors: the HOMO-LUMO energy gap (ΔE_{GAP}, equation 1) [49]; From the Koopmans' theorem [50], the ionization potential (I, equation 2) and the electron affinity (A, equation 3); According to the works of Chermette [51] and Iczkowski and Margrave [52], the electronegativity (χ, equation 4); From the Pearson's Hard and Soft Acid and Base (HSAB) theory [53] and according to the Janak theorem [54], and the work of Szentpály [55], the global hardness (η, equation 5) and the global softness (S, equation 6) introduced in the work of Yang and Parr [56]; the electrophilicity index (ω, equation 7) according to the work of Parr and Szentpály [57]; the nucleophilicity index (ε, equation 8) from the work of Chattaraj [58]. The trial version of the ChemCraft [59] software was used to render the frontier molecular orbitals.

$$\Delta E_{GAP} = E_{LUMO} - E_{HOMO} \quad (1)$$

$$I = -E_{HOMO} \quad (2)$$

$$A = -E_{LUMO} \quad (3)$$

$$\chi = \frac{I + A}{2} \quad (4)$$

$$\eta = \frac{I - A}{2} \quad (5)$$

$$S = \frac{1}{\eta} \quad (6)$$

$$\omega = \frac{\chi^2}{2\eta} \quad (7)$$

$$\varepsilon = \frac{1}{\omega} \quad (8)$$

To complete the understanding of the reactivity of chalcone, the following Fukui functions are applied: Electronic [60] (equations 9 – 12) and condensed [61] (equations 13 – 15) to the nucleophilic (f^+ and f_k^+), electrophilic (f^- and f_k^-), and radical (f^- and f_k^0) attack; and the local quantum descriptors: the dual descriptor [62] (Δf, equation 16) and the multiphilic index [63] (Δω, equation 17) to characterize the nucleophilic and electrophilic sites of the molecule. The electronic Fukui functions were obtained using the Multiwfn [64] software, and the isosurfaces were rendered using the VESTA [65] software. The molecular electrostatic potential (MEP) was computed at B3LYP/6-311++G(d,p) computational level to complete the local analysis of the chemical reactivity of the chalcone. The Gabedit program [66] was used to compute the MEP.

$$f = \left(\frac{\partial \rho(r)}{\partial N}\right)_{v(r)} \quad (9)$$

$$f^+ \approx \nu_{LUMO} \quad (10)$$

$$f^- \approx \nu_{HOMO} \quad (11)$$

$$f^0 \approx \frac{\nu_{LUMO} + \nu_{HOMO}}{2} \quad (12)$$

$$f_k^+ = q_k(N+1) - q_k(N) \quad (13)$$

$$f_k^- = q_k(N) - q_k(N-1) \quad (14)$$

$$f_k^0 = \frac{q_k(N+1) - q_k(N-1)}{2} \quad (15)$$

$$\Delta f = f_k^+ - f_k^- \quad (16)$$

$$\Delta\omega = \omega.\Delta f \quad (17)$$

Where the $q_k(N+1)$, $q_k(N)$, and $q_k(N-1)$ are the Hirshfeld charge population [67] on the atom k of the anionic, neutral, and cationic species.

Finally, the UV-Vis spectrum was calculated using the Time-Dependent Density Functional Theory (TD-DFT) using the CAM-B3LYP [51] at 6-311++G(d,p) level of theory in ethanol as an implicit solvent and the electronic transition was assignment using the GaussSum 3.0.1 [68, 69].

2.4 Assays for modulation of the antibiotic resistance and evaluation of efflux pump inhibition by MIC reduction

Antimicrobial activity of the chalcone was evaluated against *S. aureus* K2068, which are resistant to ciprofloxacin due to overexpression of the MepA genes encoding the MepA efflux pumps. The SA-K2068 strains were provided by Dr. Glenn W. Kaatz, John Dingell VA Medical Center, Detroit, MI, USA. Evaluation of the modulatory effect on the resistance to antibiotics was performed according to previously described [70]. Briefly, 150 µL of each suspended bacterial inoculum in saline solution, corresponding to 0.5 of the McFarland scale, were added to microtubes (2mL) together with 1350 µL of Brain heart infusion (BHI) as a control. In tests, 150 µL of each suspended bacterial inoculum in saline solution, corresponding to 0.5 of the McFarland scale, were added together with EPIs (MIC/8) and completed with brain heart infusion. These were then transferred to 96-well microtiter plates, and 100 µL of the antimicrobial drug and ethidium bromide serial dilutions were performed (1:1). The plates were incubated at 37 °C for 24 h, and bacterial growth was assessed by using resazurin. MIC was defined with antibiotics and ethidium bromide concentrations ranging from 0.5 to 512 µg/mL. The MIC of controls was assessed using the antibiotics and ethidium bromide alone [71].

2.5 Docking procedure

The MepA model was generated by retrieving the protein sequence for the NCTC 8325 strain from the Uniprot database. Then, the SWISS-MODEL [72] service was used to build the homology model. Of all the 50 templates generated, the one with the best Global Model Quality Estimation score was based on the structure of the multidrug and toxic compound extrusion transporter of the Bacillus halodurans (PDB-ID: 5C6N). For the docking procedure, which was carried out using the Autodock Vina [73] software, the grid box was defined as a 126Åx126Åx126Å box around the geometrical center of the model, with spacing = 0.431 e exhaustiveness = 8. Partial Gasteiger charges were added to ligand atoms, non-polar hydrogen atoms were mixed while all other parameters were kept at their default values. The best results were chosen based on the binding score.

2.6 Evaluation of physicochemical properties and drug-likeness criteria

Calculations of physical and chemical properties, which include acid dissociation constant (pKa), molecular weight (MW), consensus partition coefficient (Clog P), hydrogen bond donor (HBD) and acceptor (HBA) count, distribution coefficient at pH 7.4 (log $D_{pH7.4}$), solubility coefficient at pH 7.4 (log $S_{pH7.4}$), topological polar surface area (TPSA), number of rotatable bonds (Nrot) were performed using the plugins provided in the MarvinSketch® code [74]. To validate the "drug-likeness" criteria [75], the bioavailability radar was used, generated on the SwissADME web-server [76], which uses an algorithm based on a filter that combines the descriptors of the "rule of five" of Lipinski et al. [75] (MW≤500, log P≤5, H-bond donors≤5 e H-bond acceptors≤10) and the rule by Veber et al., (2002)[7] (TPSA≤140 e rotatable bonds≤10), establishing the parameters of lipophilicity (-0.7<log P<5.0), size (150g/mol<MW<500g/mol), polarity (20Å²<TPSA<130Å²), insolubility (-6<log S<0), unsaturation (0.25<Fraction Csp3<1) and flexibility (0<Num. Rotatable bonds<9) as a determining spatial spectrum for good oral bioavailability.

2.7Virtual screening of pharmacokinetics properties

Molecular descriptors of structure-activity relationship (QSAR) of the properties of absorption, distribution, metabolism, and excretion (ADME) were used to evaluate the pharmacokinetic behavior of chalcone. Through the MW, log P, and TPSA descriptors,

statistical evaluation was made for the models of human intestinal absorption (HIA) [77], human adenocarcinoma colon cells permeability (Caco-2) [78], blood-brain barrier penetration (BBB) [79] and P-glycoprotein substrate (Pgp) [80].

2.8 Evaluation of the multi-target bioactivity

To evaluate bioactivity, the code SMILES [COc2ccc(C=CC(=O)c1c(O)c(OC)c(OC)cc1OC)cc2] was generated, using the plug-in JSME molecular editor [81], deployed on the web-server Molinspiration (https://molinspiration.com/) and submitted to interaction simulation with main human biological targets: G-protein coupled receptor (GPCR), ion channel modulator, a kinase inhibitor, nuclear receptor ligand, protease inhibitor, and enzyme inhibitor. The simulation is based on the test of similarity of the "drug-likeness" properties of known compounds deposited in the server database, and the results are available in scores, where values above 0.5 indicate strong interaction with the specified target, between 0.2 and 0.5 moderate interactions and for values less than 0.2 low interaction potential.

2.9 Acute oral toxicity prediction model

For the prediction of Acute oral toxicity, the LabMol web-server LabMol (http://stoptox.labmol.com.br) was used, which has its algorithm based on the structure-activity relationship (QSAR) of the acute oral toxicity model in bees, meeting the guidelines of the Organization for Economic Cooperation and Development (OECD) and the Registration, Evaluation, Authorization, and restriction of chemical substances (REACH). For this test, results with a confidence index of 70% have closer proximity to the acute toxicity indexes in bees and are expressed in a contribution map by the toxic fragments, where the green-colored region is the positive contribution and the region colored red the negative contributions to this class of toxicity.

2.10 Statistical Analysis

All bacteriological tests were performed in triplicates. Data were analyzed using a two-way ANOVA followed by Bonferroni's post-hoc test (where $p<0.05$ was considered

significant). The geometric mean of the triplicates was used as the central data ± standard error of the mean. The GraphPad Prism 5.0 statistical program was used for the analysis.

3. Results and discussion

3.1 Conformational analysis

Chalcones may exist in two isomeric forms, *E*- (*trans*) or *Z*- (*cis*). The *E*-isomer is the thermodynamically most stable form in most cases [82]. The title chalcone possesses the *trans* form. It is clearly known that there are differences in the structural conformations of chalcones, especially between some of their dihedral angles [83].

The relaxed PES scan of the title chalcone calculated at the B3LYP/6-311++G (d,p) level for the dihedral angle θ (C6-C1-Cβ-Cα) with step variation of 15° is shown in Figure 1. The dashed red line in the plot in this figure corresponds the zero energy. The potential energy curve shows three minimum energy structures, two global minima around -180 ° and + 180 °, and a local minimum at 0°. The conformations at -180 ° and + 180 are equivalent, and correspond the configurations I and III, while the conformation at 0° corresponds the configuration II. According to our calculation, the configuration I is more stable than configurations II and III by 1.23 kJ/mol. It is also noted that the conformers I, II and III presented the isomeric form *E*- (*trans*). Figures. 2 shows the lower energy conformers of the title chalcones.

3.1 NMR data

The ^{1}H NMR spectrum of this chalcone showed signals at δ_H 3.78 - 3.91 ppm relative to the hydrogens of methoxy groups. These signals can also be observed in the ^{13}C NMR spectrum at δ_C 55.5 to 60.9 ppm. The signals at δ_H 7.24 and 7.75 ppm (J = 14.6 Hz) were attributed to doublets referring to α,β-unsaturated hydrogens, whose coupling constant (J) confirms the stereochemistry *E*, in the ^{13}C NMR, these signals are observed at δ_C 142.9 (Cβ) and 128.4 (Cα) being related to olefinic carbons α and β, respectively. The singlet observed at δ_H 5.93 ppm refers to hydrogen attached to the carbon 5' whose signal is observed at δ_C 87.3ppm in the ^{13}C NMR spectrum. The signal at δ_C 193.3 ppm concerns to

α,β-unsaturated carbonyl group. The ketone absorbs 203.8 ppm, however, the presence of α, β unsaturation, causes a displacement to the high field, and the probable cause is the delocalization of charge by the benzene ring or by the double bond that makes carbonyl carbon less electron deficient. In addition, the signs at δ_C 159.5 (C-4´), 158.7 (C-2´), 158.6 (C-6´), 130.3 (C-3´), and 107.1 (C-1´) refer to the non-hydrogenated carbons present in ring A of the chalcone. The signals at δ_H 7.53 (d, *J* = 8.4 Hz, H-2/6) and 7.89 ppm (d, *J* = 8.4 Hz, H-3/5) are related to the signs at 125.2 (C-2/6) and 130.3 (C-3/5) in the ^{13}C NMR spectrum, and the signs at δ_C 131.0 (C-4) and 130.7 ppm (C-1) refer to the non-hydrogenated carbons present in ring B (Table 1). This chalcone has two aromatic rings linked by a three-carbon α,β-unsaturated carbonyl system. The ring A is formed by the atoms C1′, C2′, C3′, C4′, C5′ and C6′, and the ring B is formed by the atoms C1, C2, C3, C4, C5, and C6. The molecule was drawn according to this experimental result, and the geometrical optimization calculation carried out using the B3LYP/6-311++G(d,p) computational level in chloroform as an implicit solvent. The optimized structure for the chalcone is shown in Figure 2. The ^{1}H and ^{13}NMR were theoretically calculated at the same level of theory as the optimization. The theoretical results for the calculated chemical shift were displaced in Table 1. To understand the correlation between the experimental and theoretical data, the linear fitting was made using the experimental and calculated chemical shifts for the ^{1}H and ^{13}C NMR (Figure 3). The linear correlation was computed with the coefficient of determination (R^2) of 0.98669 with the linear equation of y = 0.94812x + 0.77857. This result shows an excellent agreement between the experimental and theoretical data; hence the chalcone had its molecular structure confirmed to be the same as in Figure 2.

The molecular structure of the chalcone was described to the in the global minimum of energy due to the absence of any imaginary frequency in the vibrational spectrum; hence the simulated molecule describes the real molecule of the chalcone. The molecule is not planar: the ring A is about 54.161° out of the plane delimited by the α,β-unsaturated carbonyl. The O18, C8, Cα, and Cβ structure (α,β-unsaturated carbonyl) is almost planar with a little deviation of -1.081°. The ring B is in the same plane as the structure previously describes with an angle of only 0.112°. The four methoxy groups showed bond length for the carbon (ring)-oxygen sigma bond of 1.38151 Å (C3′-O27), 1.35811 Å (C4′-O28),

1.36371 Å (C6′-O24), and 1.35837 Å (C4-O41). The hydroxyl group showed a bond length of 1.35693 Å (C2′-O23), and the carbonyl group value of 1.22753 Å (C8-O10). The π-bond between the carbon atoms Cα and Cβ demonstrate the bond length of 1.34848 Å, and the bonds Cα-H12 and Cβ-H14 the values respectively of 1.08240 Å and 1.08747 Å. The bonds C8-C1′, C8-Cα, and Cβ-C1 have a bond length of 1.50254 Å, 1.47647 Å, and 1.45611 Å, respectively. For the methyl groups, the bond lengths are 1.44312 Å (O27-C29), 1.09379 Å (C29-H31), 1.08916 Å (C29-H30), and 1.09052 Å (C29-H32); 1.42931 Å (O28-C33), 1.08798 Å (C33-H34), 1.09370 Å (C33-H35), and 1.09349 Å (C33-H36); 1.42683 Å (O24-C37), 1.08816 Å (C37-H38), 1.09408 Å (C33-H39), and 1.09397 Å (C37-H40); 1.42929 Å (O41-C42), 1.08794 Å (C42-H43), 1.09377 Å (C42-H44), and 1.09375 Å (C42-H45). For the ring A, the unique C-H bond showed a bond length of 1.07783 Å. For the ring B, the four C-H bonds have the bond length of 1.08345 Å (C2-H21), 1.08352 Å (C3-H22), 1.08129 Å (C5-H25), and 1.08486 Å (C6-H20). Finally, the carbon-carbon bonds in the rings A and B are described by the following bond lengths: for the 1.40420 Å (C1′-C2′), 1.39896 Å (C2′-C3′), 1.39864 Å (C3′-C4′), 1.39976 Å (C4′-C5), 1.39723 Å (C5′-C6′), and 1.40792 Å (C6′-C1′) respectively in the ring A; for the 1.41173 Å (C1-C2), 1.38091 Å (C2-C3), 1.40589 Å (C3-C4), 1.39800 Å (C4-C5), 1.39287 Å (C5-C6), and 1.40295 Å (C6-C1) respectively for ring B.

Finally, the thermodynamics properties were computed at 298.15 K and 1 atm of pressure to complete the structural description of the chalcone using B3LYP/6-311++G(d,p) computational level in chloroform as an implicit solvent. The calculated values of the thermodynamic properties Internal Energy (U), the Heat Capacity at constant volume (C_v), Enthalpy (H), Entropy (S), and Gibbs Free Energy (G) were respectively 239.639 kcal.mol^{-1}, 92.406 cal.mol^{-1}K^{-1} 703.771 kcal.mol^{-1}, 175.04 cal.mol^{-1}.K^{-1}, and 651.583 kcal.mol^{-1}. The Zero-Point Energy (ZPE) and the Electronic Energy (E_0) were respectively 223.900 kcal.mol^{-1} and -1,187.683697 Hartree. For comparison, the thermodynamics properties Internal Energy, Enthalpy, Entropy, and Gibbs Free Energy for the chalcones previously studied [17, 38] are respectively 181.231 kcal.mol^{-1}, 532.4667 kcal.mol^{-1}, 148.9 cal.K^{-1}mol^{-1}, and 488.072 kcal.mol^{-1} for the PAAPFBA chalcone [17]; 239.837 kcal.mol^{-1}, 704.866 kcal.mol^{-1}, 173.234 cal.K^{-1}mol^{-1}, and 653.217 kcal.mol^{-1} for the cinnamaldehyde chalcone [38]. The molecular structure of the chalcone is more similar

to the cinnamaldehyde chalcone; hence the values for the thermodynamics properties are similar. However, the PAAPFBA chalcone has a fluorine atom bonded in ring B and an acetamide group bonded in ring A and the values for the same properties are different from the values obtained to the HPHENYL and cinnamaldehyde chalcones, which shows how the ligands in both phenyls ring A and B can change the properties of the entire molecule.

3.2 Infrared analyses

The ATR-IR absorbance spectrum of the chalcone is presented in Figure 4. We highlighted 18 bands in the infrared spectrum, assigned with the help of the DFT calculations, and listed in Table 2. The linear fitting was made using those highlighted infrared bands. The result is shown in Figure 5. The coefficient of determination (R^2) has a value of 0.99812, with the linear equation y = 0.9945x + 5.9665. This result shows an excellent agreement of the experimental values and the theoretical wavenumbers. Therefore, the theoretical model for the liquid phase using chloroform as solvent is reliable and complement the understanding of the ATR-FTIR spectrum of the title chalcone. Infrared spectra of 2-bromo-4-chlorobenzaldehyde in solid phase and in n-hexane, cyclohexane, chloroform, benzene, toluene as non-polar solvents and ethanol, 2-propanol, methanol as polar solvents were investigated by Parlak and Ramasami [84]. They showed that the theoretical infrared spectra in solutions show excellent agreement with the experimental data in solid phase, mainly for the carbonyl stretching mode.

The bands of wavenumbers at 3119, 2933, and 2832 cm^{-1} in the experimental infrared spectrum of the title chalcone are associated with stretching modes of the groups, CβH14 (97%), asymmetrical stretching in the methyl group C37H39 (48%) and C37H40 (51%), and symmetrical stretching of the methyl group C37H39 (46%) and C37H40 (44%), respectively, whereas the infrared band at 1619 cm^{-1} is associated with the mixture of carbonyl stretching mode (C8=O18) with Cα-Cβ stretching mode. The C-C stretching modes of the ring B are observed in the infrared spectrum at 1547 cm^{-1} with the movement of the atoms C4-C5 mainly (PED = 21%) and the CαCβ stretching (PED = 12%).

The ATR-IR absorbance bands observed at 1507 cm^{-1} corresponds to a combination of the bending modes of the H21C2C3 (14%), H20C6C5 (14%), H22C3C4 (14%), and H26C5C6 (15%), whereas the infrared band at 1468 cm^{-1} corresponds to the bending modes

of the H39C37H38 (16%), H34C33H36 (22%), H35C33H34 (29%), H38C37H40 (30%). The more intense infrared band located at 1415 cm^{-1} is associated with the stretching modes of the C3′C2′ (16%), C2'C1' (16%), O23C2′ (18%) in ring A. At 1333 and 1290 $cm^{-1,}$ there are mixed vibrational modes for the bending and stretching of the following group of atoms respectively: H21C2C3 (10%), H12CαCβ (11%), H14CβCα (15%), and CβCα (11%) at 1333 cm^{-1}; H21C2C3 (11%), H14CβCα (18%), and CβC1′ (14%) at 1290 cm^{-1}. The band at 1210 cm^{-1} is associated with the bending and stretching modes of the groups H7C5′C4′ (14%) and O27C3′ (26%), respectively. Stretching modes of the carbon-oxygen bonds O28C33 (11%) and O28C4′ (17%) are observed in the band at 1151 cm^{-1}. A strong infrared band, which is associated with the stretching of the methoxy group O24C37 (16%), O23C2′ (20%), is observed at 1117 cm^{-1}. Stretching and bending modes of the O27C29 (23%), C4C5C6 (12%), and C2C3C4 (21%) are observed at 992 cm^{-1}.

At 828 cm^{-1} it was observed mixed modes between the out of plane deformations and two torsions respectively in the ring B for the group of atoms O41C3C5C4 (10%), H22C3C4C5 (10%), and H21C2C3C4 (13%). Out of plane deformation and torsion of the ring A respectively are observed in the wavenumbers 678 (O28C5′C3′C4′ with PED = 13% and O24C5′C1′C6′ with PED = 14%) and 588 cm^{-1} (H25O23C2'C3' with PED = 82%), whereas the mode at 425 cm^{-1} has low intensity and corresponds to bending modes of the C33O28C4′ (13%) and C6C1Cβ (15%). Therefore, the vibrational analysis allowed us to obtain information on the main infrared bands of the chalcone.

3.3 Electronic Properties analysis

The Frontier Molecular Orbitals (FMO) for the title chalcone were calculated using the B3LYP/6-311++G(d,p) computational level, and they are shown in Figure 6. The Highest Occupied Molecular Orbital (HOMO) is related to the molecule's ability to donate electronic density (nucleophilic character), while the Lowest Unoccupied Molecular Orbital (LUMO) is related to the molecule's ability to accept electronic density (electrophilic character). The HOMO is mainly spread over the phenyl group of the ring A due to the π-bonds, also is spread over the oxygen atoms of the methoxy groups (O24, O27, and O28), in the π-bond between the carbon atoms CαCβ, in the oxygen atom (O18) of the carbonyl

group, in the π-bonds of the phenyl group in the ring B, and in the oxygen atom (O41) of the methoxy group. Besides, the LUMO is mainly spread over the π* antibonding positions of the phenyl group in the ring B, the bond between the CαCβ, and the oxygen atom (O18) of the carbonyl group. There is a little contribution of the π* antibonding for the ring A. Hence, the region of the molecule responsible for donating electronic density is the ring A, the ring B, and the olefin group (CαCβ), while the region responsible for accepting electronic density is the ring B and the α,β-unsaturated carbonyl group. The electronic transition between the HOMO and the LUMO is $\pi \rightarrow \pi^*$.

To understand the chemical behavior of the chalcone, the quantum reactivity descriptors were computed at the same level of theory from the energies values of the HOMO and the LUMO, and they are shown in Table 3. The values of the quantum descriptors show that the title chalcone has an electrophilic character due to the higher values of the electronegativity and the electrophilicity index. The LUMO as a spread over the entire molecule, the extra negative charge. Besides, the molecule has a high ionization potential, which means it is difficult to donate electronic density. This result is confirmed by the low value of the nucleophilicity index. The molecule can be classified as a hard molecule due to the high value of the global hardness in comparison with the global softness and the high value of the energy gap, which agrees with the difficulty of electronic-donation of this molecule. Therefore, the chalcone should interact better with substrates that have a good electronic donation character. Also, in Table 3 is shown the comparison of the quantum reactivity descriptors computed for the chalcone and the PAAPFBA [17] and cinnamaldehyde [38] chalcones. The chalcone should be more reactive than the PAAPFBA and should be less reactive than the cinnamaldehyde chalcone due to the values of the HOMO-LUMO energy gap. The chalcone has a lower value of electronegativity; hence this molecule also has the lower electrophilic character, consequently the higher nucleophilic character, which is proved by the higher value of the energy value for the HOMO when compared to the others chalcones.

3.4 Fukui functions and local reactivity descriptors analysis

The Fukui functions (Electronic and Condensed) are used to understand how each atom behaves during a chemical reaction. The quantum reactivity descriptors give an

overview of the molecule's reactivity; however, the Fukui functions together with the dual descriptor (Δf) and the multiphilic index (Δω), a more selective analysis can be made on each atom.

The Electronic Fukui functions for the nucleophilic attack (f^+), electrophilic attack (f^-), and radical attack (f^0) are shown in Figure 7. The green and the blue colored represent the positive and the negative signs of the Fukui functions, respectively. The higher the value of the Fukui function, the higher the propensity for the determined attack (nucleophilic, electrophilic, or radical). For the nucleophilic attack, the most susceptible atoms are Cα, Cβ, O18, C2, C4, C6, and O41. In this case, the molecule behaves like an electrophilic site; hence the f^+ function is related to the LUMO. These atoms have mainly the LUMO spread over them; hence they are most prone to accept electronic density. For the electrophilic attack, the most susceptible atoms are C1, C2, C3, C4, C5, C6, C8, O41, Cα, Cβ, O18, C1′, C3′, O24, and O28. The f^- function is related to the HOMO because the molecule behaves as a nucleophilic site. Despite a larger number of atoms that are susceptible to donate electronic density, this molecule has a low energy level for the HOMO and higher ionization potential due to the more delocalization of the electronic density within the molecule. For the radical attack (f^0), the most susceptible atoms are C1, C2, C3, C4, C5, C6, O41, Cα, Cβ, O18, C1′, C2′, C3′, and the hydrogen atoms. The carbon and oxygen atoms can stabilize the radical due to the resonance effect, and the hydrogen atoms are lost during the reaction between a radical species.

The results from the calculations of the Condensed Fukui functions, dual descriptor, and multiphilic index are shown in Table 4. The Condensed Fukui functions were computed from the Hirshfeld charge analysis [67] for the anionic (N+1), neutral (N), and cationic (N-1) species of the title chalcone. According to the results, for a nucleophilic attack, the most susceptible atoms are C2′, C5′, C1, C2, C3, C4, C5, C6, O24, O27, C33, and C37. For the electrophilic attack, the most propensity atoms are C1′, C2′, C4′, C5′, C6′, C8, C2, O27, C29, C37, and C42. For the radical attack, the most susceptible atoms are C1′, C2′, C4′, C5′, C6′, C1, C3, C5, O24, O27, O28, C29, C33, C37, and C42. The relation between the Condensed Fukui functions and the local reactivity descriptors (the dual descriptor and the multiphilic index) lies in the following fact: if both Δf and Δω are positive, the reactive site has an electrophilic character, and if Δf and Δω are negative, the

reactive site has nucleophilic character. The values in Table 4 show that the electrophilic sites are in atoms C1′, C2′, C3′, C4′, C5′, C6′, C1, C3, C5, O24, O27, O28, C29, C33, C37, O41, and C42. The nucleophilic sites are in the atoms C8, Cα, Cβ, O18, C2, C4, and C6. The negative values for the condescended Fukui functions confirm the analysis made by the Electronic Fukui Functions that the HOMO is not too available to donate electronic density since the electronic density is spread over the entire molecule due to the resonance effect, hence due to the higher nucleophilic character of the chalcone when compared to the PAAPFBA [17] and cinnamaldehyde [38], the title chalcone can use the inner molecular orbitals (HOMO-1, HOMO-2, etc.) to donate electronic density during a nucleophilic attack [85, 86].

3.5 Molecule Electrostatic Potential (MEP)

The Molecular Electrostatic Potential (MEP) was computed at B3LYP/6-311++G(d,p) level of theory (Figure 8). The MEP has the following color scheme: the red-colored is related to a negatively charged region, the yellow-colored to a partially negative charge region, the green-colored to a neutral region, the light blue color to a partially positive region, and the blue-colored to a positively charged region. The nucleophilic sites of the molecule are displayed as red to yellow colored regions due to higher concentration of electronic density. The electrophilic sites are displayed as light blue to blue colored regions due to the electron deficient. The oxygen atoms from the carbonyl, methoxy, and hydroxyl groups, the π electrons from the phenyl rings, and the π electrons from the CαCβ bond are most susceptible to interact with positive regions of a substrate. The hydrogen atoms with a partially positive charge are most susceptible to interact with negative regions from other molecules. These results are directly related to the Fukui functions and the FMO analysis.

3.6 UV-Vis spectrum analysis

In addition, the spectrum of UV-Vis absorption of chalcone is presented in Figure 9. Analyzing this spectrum, it is possible to observe the maximum wavelength, λ_{max}, at 375 nm, which corresponds to an energy value of 3.31 eV. For the theoretical characterization,

the UV-Vis absorption spectrum was computed using the Time-Dependent Density Functional Theory (TD-DFT) at CAM-B3LYP/6-311++G(d,p) level of theory in ethanol media. The calculated UV-Vis spectrum is shown in Figure 10. The maximum value for the absorption wavelength was found at 333.10 nm, which correspondent energy of 3.7221 eV with an oscillator strength of 0.5846. The electronic transitions which are responsible for this transition are the HOMO-2→LUMO (6%), the HOMO-4→LUMO (29%), and the HOMO→LUMO (56%). Hence, the absorption band in the experimental UV-Vis spectrum of the chalcone is described mainly for the $\pi \rightarrow \pi^*$ transition between the HOMO and the LUMO, and the difference between the experimental and theoretical maximum wavelength is less than 50 nm.

3.8 Evaluation of the major microspecies

By analyzing the calculated pKa value of chalcone in the order of 7.76, it is possible to observe the chemical balance between the microspecies of the molecular system of the substance. The graph expressed in Figure 11 shows the distribution of chalcone microspecies as a function of pH variation, where it is worth noting that the loaded species is formed close to the physiological pH levels (approximately 7.4), since the blue curve shows a trend decreasing the concentration of the neutral species of the compound, while the concentration of the ionic species shown by the orange curve tends to 100%. Considering the relations established by the Henderson–Hasselbalch equation and the calculated value compatible with experimental data from other phenolic hydroxyls, at the time when pH> pKa, the chemical equilibrium shifts towards the formation of the ionic species as the most abundant in the system, since such behavior occurs only at high basic pH levels. Thus, it was possible to identify a concentration of 69.49% associated with neutral species as the major microspecies at pH 7.4 (Figure 12).

3.9 Evaluation of the physicochemical properties

Chalcones are often mentioned in studies that relate to structure-activity (QSAR). The predicted and observed antimycobacterial, antibacterial, antituberculosis, and anticancer

biological activities show a linear trend of fidelity between theoretical molecular descriptors and the bioactivity performed by these small molecules [75, 87-89]. Directly associated with lipophilicity and permeability, important descriptors of rational drug planning such as partition coefficient between n-octanol and water (log $P_{o/w}$) e topological polar surface area (TPSA) and topological polar surface area (TPSA) can provide information on the pharmacokinetic behavior of a given substance, as well as its oral bioavailability. As a rule, most of the experimental findings involving these two properties in theoretical screens suggest that compounds with positive values of log P are associated with compounds with hydrophobic behavior and TPSA≤140Å² values with compounds capable of penetrating diverse biological membranes [76, 88, 89]. Thus, the calculated value of Clog P in the order of 3.61 indicates that chalcone is predominantly lipophilic, while its TPSA value of 74.22Å² indicates a good capacity for cell permeability (Table 5).

In the filter that combines the drug-likeness criteria of Lipinski's "rule of five" (MW≤500, log P≤5, H-bond donors≤5 and H-bond acceptors≤10) [75] and Veber's parameters (TPSA≤140 e rotatable bonds≤10) [89], the bioavailability radar shown in Figure 12 shows the ideal physicochemical properties that refine chalcone as a good candidate for an oral drug [76]. It is verifiable that, despite the violation in the unsaturation score (INSATU) of type Fsp3 <0.25, the compound does not violate any criteria of the rules of Lipinski and Veber, satisfying the conditions within the ideal spectrum that combines lipophilicity properties (LIPO), size molecular (SIZE), polarity (POLAR), flexibility (FLEX) and insolubility (INSOLU) (Figure 12).

3.10 Virtual screening of pharmacokinetics properties

In a systematic statistical analysis that relates structure to permeability, some descriptors make it possible to predict intestinal absorption of small molecules, such as the distribution coefficient (log D), which, directly related to lipophilicity (log P), indicates the absorption potential in specific pH. In these conditions, the lipophilicity indexes incorporated into the log D values between 0 and 3 are associated with compounds with good intestinal absorption. In addition, the model is used to identify anticancer compounds by permeability in Caco-2 model cells, associated with compounds with log P between 1

and 10 [77, 90]. The calculated log value $D_{pH7.4}$ 3.45 indicates that chalcone has a high intestinal absorption (Figure 13A), while the model indicates that the compound has moderate permeability potential in Caco-2 cells, which can vary from 20 -70%. In addition, it is possible to observe that the decrease in the values of log D as a function of the increase in pH implies in the reduction of the potential for absorption of the compound, behavior related to ionic species resulting from the chemical balance between the microspecies in physiological pH, at the same time in there is an increase in the solubility coefficient evaluated in log S -3.74 at pH 7.4 (Figure 13B) with a moderate concentration of approximately 0.06 mg / mL, reaching high concentrations that can reach up to 344.36 mg / mL at high pH levels (Figure 13C).

As activity in the drug distribution stage, the transport of substances in the central nervous system (CNS) is an analysis of great importance in pharmacokinetic studies, since only 15% of compounds that penetrate the blood-brain barrier (BBB) perform efflux by plasma proteins, such as P-glycoprotein (Pgp) [91]. In experimental observations made by Kelder et al. (1999) [78], compounds with TPSA values TPSA<60-70Å² are more likely to be active in the CNS by penetrating the BBB in phase II clinical tests, while the statistical observations refine compounds as substrates of Pgp those with log P> 0 and MW between 200 and 400 g / mol [79]. Through the filter that combines the two observations to describe the behavior of chalcone in the CNS, it can be observed that, despite the ellipse formed between the values of MW and Clog P showing chalcone as a substrate for Pgp, the substance has a high probability of being inactive in the CNS because it does not permeate from the BBB (Table 5).

3.11 Evaluation of the multi-target bioactivity

The prediction of toxicological effects is gaining more and more prominence in pharmacokinetic studies, especially in the identification of toxic fragments that intercalate between the cyclic structures of DNA molecules in an intracellular environment, resulting in tumorigenicity. The so-called mutagens are precursors of mutagenicity that involves the DNA structures of a host in the development of tumorigenic activity in human cells. In this context, the virtual screening by the interaction with the different human biological targets

allows to identify the carcinogenic activity of a certain chemical species [79, 92-95]. Thus, the score of interaction with the target of G-protein coupled receptor (GPCR) in the order of -0.10 associated with a low index of chalcone interaction with this target, located in the membranes of human cells, indicating minimal toxicological risk due to modification of intracellular gene pool (Table 5).

Considered one of the main ion channel modulators, the human Ether-to-go-go-Related Gene (hERG) ion transporter is associated with the electrical conduction of the system that surrounds the human heart and in the modulation of cells in the nervous system, and its inhibition results in complications such as cardiac arrhythmia and cancer events such as leukemia [96-100], where the inhibition score of -0.08 for chalcone indicates low cardiotoxic risk (Table 5).

In the stage of phase I metabolism, the cytochrome P450 (CYP450) isoenzymes, in particular the CYP3A4 and CYP2C9 enzymes, play a fundamental role in the biotransformation of drugs through O- type oxidation reactions [101]. Physico-chemical properties such as log $D_{pH7.4}$ and log P are related to CYP450 substrates since the sites of interaction with these enzymes are predominantly lipophilic [102]. The positive values of log $D_{pH7.4}$ and log P suggest that chalcone interacts as a substrate of the main CYP450 isoenzymes, while the inhibition score of them evaluated at 0.02 indicates the low probability of inhibitory actions of these isoenzymes, indicating that the compound is subject to drug modifications by oxidation of the phenolic hydroxyl (Table 5).

Figure 13D shows the contributions of the structure-activity relationship (QSAR) to the chalcone acute oral toxicity model. In this model, the green-colored area represents the positive contributions to the toxicity model, showing the non-toxic molecular fragments, while the red-colored region indicates the negative contributions. Thus, the toxicity model of the test indicates, with a 70% reliability index, that the minimum oral dose administered does not result in toxicity.

3.12 Potential Antibacterial Activity and Evaluation of Efflux Pump Inhibition

The modulating effect of the chalcone on the resistance of the SA-K2068 strain to ciprofloxacin can be seen in Figure 14. It can be seen that the addition of chalcone in

subinhibitory concentrations to the growth medium caused a reduction of the MIC values for ciprofloxacin strain. The synergic effect presented by the chalcone was the same as the modulating effect observed for CCCP, which is cited in the literature as an inhibitor of the MepA efflux pump [71]. This effect against the MepA efflux pump is due to the inhibition of the efflux pump mechanism, which can be proven by similar behavior observed examining the association of this chalcone with ethidium bromide (Figure 14). Previous studies showed a similar effect when the DB Thiphene chalcone was tested for the SA-K2068 strain. DB Thiophene showed a better inhibition potential for CCCP-sensitive efflux pumps than the standard inhibitor, also acting as a strong inhibitor of efflux pumps in the Ciprofloxacin test [71].

3.13 Docking Results

In order to better understand the MepA inhibition mechanism displayed by the chalcone, a docking essay was carried out. Both the chalcone and ciprofloxacin were individually docked against a MepA model. Figure 15 shows the best poses of both molecules docked on the binding site of the MepA mode; as can be clearly seen from the figure, the chalcone docks to the model in almost the same way as the antibiotic. It also interacts with essentially the same residues. Figure 16 shows the two-dimensional map of the interactions between the title chalcone and the MepA model. Despite of the HOMO is mainly spread over the ring A, the ring B makes a π interaction with the amino acids methionine (MET 142) and phenylalanine (PHE 62) since this chalcone has electronic density to donate, and the LUMO is mainly spread over the ring B; hence this chalcone can also receive electronic density from the amino acids.

The binding energy of the best pose of chalcone was -6.8kcal/mol. Although the binding energy is essentially a ranking system for the poses of the ligand, one could use it to compare affinities to the model, provided the ligands being compared have similar molecular weights. With that caveat in mind, the binding energy of the ciprofloxacin antibiotic was -7.6kcal/mol. The slightly higher affinity of ciprofloxacin could be attributed to the hydrogen bond between the antibiotic and the Asn205 residue, which is shorted than the hydrogen bond between chalcone and Gln284. Also, these binding energies are not only

close to each other, but also on par with those reported on the literature for MepA and NorA models. Rezende-Júnior et al. [103] have reported that the binding energies of several chalcones to a NorA model are approximately 7 kcal/mol.

4. Conclusion

The analyses allowed drawing the molecular structure of the chalcone synthetized with subsequent confirmation using the quantum chemical calculations with an excellent linear correlation between the experimental and theoretical chemical shifts. The spectroscopic analysis allowed obtaining information of the main infrared bands of chalcone, and together with the theoretical assignments of the vibrational modes of those band, the Infrared spectroscopic analysis contributed to confirm the molecular structure of chalcone, and the electronic characterization identified the regions of the molecule that are responsible to donate (nucleophilic) and to accept (electrophilic) electronic density. The drug-likeness criteria based on the rules of Lipinski and Veber evaluated that the compound has the ideal physicochemical properties for the realization of its active ingredient as an oral drug, and the low interaction with plasma proteins indicates a molecular fraction of the bioavailable substance for interactions with specific biological targets in docking tests and molecular dynamics. The molecular size and lipophilicity models suggest that the substance has a high probability of being an inactive drug in the CNS, and its transport by Pgp indicates that there is no risk of toxicity due to residual drug accumulation in the blood. The structure-activity relationship (QSAR) of chalcone and the low rates of interaction with the targets GPCR and Ion CM suggest that the minimum oral dose administered does not present a toxic risk to the nervous system and the respiratory system, constituting a good candidate for drug orally. In addition, the microbiological tests show that the chalcone can be used as a possible inhibitor of the Mep A efflux pump, also revealing that chalcone can be used as a base for the design of substances with antibiotic modifying activity.

CRediT authorship contribution statement

Jayze da Cunha Xavier: Investigation. Data curation. Formal analysis, Writing - original draft. **Francisco W. Q. Almeida-Neto:** Software, Validation, Formal analysis. **Priscila T.**

da Silva: Data curation. **Amanda P. de Sousa:** Data curation. **Emmanuel S. Marinho:** Formal analysis, Writing—review and editing, **Márcia M. Marinho:** Formal analysis, Writing—review and editing. **Janaina E. Rocha:** Methodology. **Priscila R. Freitas:** Methodology. **Ana C. J. de Araújo:** Methodology. **Thiago S. Freitas:** Methodology. **Carlos E. S. Nogueira:** Software, Formal analysis, Writing—review and editing. **Pedro de Lima-Neto:** Conceptualization. **Paulo N. Bandeira:** Conceptualization, Resources. **Alexandre M. R. Teixeira**: Formal analysis, Funding acquisition. **Henrique D. M. Coutinho:** Methodology, Resources. **Hélcio Silva dos Santos:** Supervision, Project administration, Formal analysis, Writing—review and editing.

Declaration of competing interests

The authors declare that they have no known competing financial interests or personal relationships that could have appeared to influence the work reported in this paper.

Acknowledgments: The authors thank FUNCAP, CAPES, and CNPq for financial support and scholarship. A.M.R. Teixeira acknowledges the financial support from the CNPq (Grant#: 305719/2018-1). The authors also thank Centro Nacional de Processamento de Alto Desempenho (CENAPAD) of the Federal University of Ceará (UFC) for providing computational resources. Thanks to the India government program "Research Training Fellowship for Developing Country Scientist" (RTF-**DCS/2019/000192**).

References

[1] D.E. Payne, B.R. Boles, Emerging interactions between matrix components during biofilm development, Current Genetics, 62 (2016) 137-141. https://doi.org/10.1007/s00294-015-0527-5.

[2] M. Jamal, W. Ahmad, S. Andleeb, F. Jalil, M. Imran, M.A. Nawaz, T. Hussain, M. Ali, M. Rafiq, M.A. Kamil, Bacterial biofilm and associated infections, Journal of the Chinese Medical Association, 81 (2018) 7-11. https://doi.org/10.1016/j.jcma.2017.07.012.

[3] S.J. Dancer, The effect of antibiotics on methicillin-resistant Staphylococcus aureus, Journal of Antimicrobial Chemotherapy, 61 (2008) 246-253. https://doi.org/10.1093/jac/dkm465.

[4] F. Aqil, I. Ahmad, M. Owais, Evaluation of anti-methicillin-resistant Staphylococcus aureus (MRSA) activity and synergy of some bioactive plant extracts, Biotechnology Journal, 1 (2006) 1093-1102. https://doi.org/10.1002/biot.200600130.

[5] H.D.M. Coutinho, J.G.M. Costa, E.O. Lima, V.S. Falcao-Silva, J.P. Siqueira, Jr., Enhancement of the antibiotic activity against a multiresistant Escherichia coli by Mentha arvensis L. and chlorpromazine, Chemotherapy, 54 (2008) 328-330. https://doi.org/10.1159/000151267.

[6] S. Krishna, L.S. Miller, Host-pathogen interactions between the skin and Staphylococcus aureus, Current Opinion in Microbiology, 15 (2012) 28-35. http://dx.doi.org/10.1016/j.mib.2011.11.003.

[7] P.M. Dugourd, A. Dupont, T. Hubiche, C. Chiaverini, A. Alkhalifa, L. Roudiere, A. Tristan, C.A. Gustave, P. Del Giudice, Staphylococcal toxic shock syndrome should be considered in the event of diffuse erythema with fever and shock, Annales de Dermatologie et de Venereologie, 146 (2019) 287-291. https://doi.org/10.1016/j.annder.2018.12.002.

[8] S.P. Bergin, T.L. Holland, V.G. Fowler, S.Y.C. Tong, Bacteremia, Sepsis, and Infective Endocarditis Associated with Staphylococcus aureus, in: F. Bagnoli, R. Rappuoli, G. Grandi (Eds.) Staphylococcus aureus: Microbiology, Pathology, Immunology, Therapy and Prophylaxis, Springer International Publishing, Cham, 2017, pp. 263-296.

[9] P.M. Wright, I.B. Seiple, A.G. Myers, The Evolving Role of Chemical Synthesis in Antibacterial Drug Discovery, Angewandte Chemie-International Edition, 53 (2014) 8840-8869. https://doi.org/10.1002/anie.201310843.

[10] M.T.A. Oliveira, A.M.R. Teixeira, H.D.M. Coutinho, I.R.A. Menezes, D.M. Sena, H.S. Santos, B.M. de Mesquita, M.R.J.R. Albuquerque, P.N. Bandeira, R. Braz-Filho, Identification and Modulatory Activity Assessment of 2-Hydroxy-3,4,6-trimethoxyacetophenone Isolated from Croton anisodontus Mull. Arg.(Euphorbiaceae), Natural Product Communications, 9 (2014) 1934578X1400900520. http://dx.doi.org/10.1177/1934578X1400900520.

[11] P.H.M. Torres, A.C.R. Sodero, P. Jofily, F.P. Silva-Jr, Key Topics in Molecular Docking for Drug Design, International Journal of Molecular Sciences, 20 (2019). https://doi.org/10.3390/ijms20184574.

[12] S. Saikia, M. Bordoloi, Molecular Docking: Challenges, Advances and its Use in Drug Discovery Perspective, Current Drug Targets, 20 (2019) 501-521. https://doi.org/10.2174/1389450119666181022153016.

[13] D.G. do Rego, B.G. de Oliveira, Um Estudo Químico-quântico da Covalência Intermolecular em Sistemas Estabilizados por Ligações de Hidrogênio π··· H e N··· H: Cálculos DFT, ChelpG, NBO e QTAIM, Orbital: The Electronic Journal of Chemistry, 1 (2016) 1-11.

[14] S. Burmaoglu, S. Ozcan, S. Balcioglu, M. Gencel, S.A.A. Noma, S. Essiz, B. Ates, O. Algul, Synthesis, biological evaluation and molecular docking studies of bis-chalcone derivatives as xanthine oxidase inhibitors and anticancer agents, Bioorganic Chemistry, 91 (2019) 103149. https://doi.org/10.1016/j.bioorg.2019.103149.

[15] S. Burmaoglu, E.A. Kazancioglu, R. Kaya, M. Kazancioglu, M. Karaman, O. Algul, I. Gulcin, Synthesis of novel organohalogen chalcone derivatives and screening of their molecular docking study and some enzymes inhibition effects, Journal of Molecular Structure, 1208 (2020) 127868. https://doi.org/10.1016/j.molstruc.2020.127868.

[16] P. Yadav, J.K. Yadav, A. Agarwal, S.K. Awasthi, Insights into the interaction of potent antimicrobial chalcone triazole analogs with human serum albumin: spectroscopy and molecular docking approaches, RSC Advances, 9 (2019) 31969-31978. https://doi.org/10.1039/C9RA04192C.

[17] F.W.Q. Almeida-Neto, L.P. da Silva, M.K.A. Ferreira, F.R.S. Mendes, K.K.A. de Castro, P.N. Bandeira, J.E.S.A. de Menezes, H.S. dos Santos, N.K.V. Monteiro, E.S. Marinho, P. de Lima-Neto, Characterization of the structural, spectroscopic, nonlinear optical, electronic properties and antioxidant activity of the N-{4'-[(E)-3-(Fluorophenyl)-1-(phenyl)-prop-2-en-1-one]}-acetamide, Journal of Molecular Structure, 1220 (2020) 128765. https://doi.org/10.1016/j.molstruc.2020.128765.

[18] P.T. Silva, L.L.M. A., J.C. Xavier, M.C.S. Carvalho , M.O. Moraes, C. Pessoa, F.W.A. Barros, P.N. Bandeira, C.S.P. Cavalcante, A.M.R. Teixeira, R.O.S. Fontenelle, H.S. Santos, Atividade Citotóxica e Antifúngica de Chalconas Sintetizadas a partir de uma Acetofenona Natural Isolada de Croton anisodontus, Revista Virtual de Química, 12 (2020) 712-723. https://doi.org/10.21577/1984-6835.20200057.

[19] P.T. Silva, T.S. Freitas, D.M. Sena, Jr.; , P.N. Bandeira, M.S.S. Julião, E.S. Marinho, A.A.C. Alcanfor, E.M. Marinho, P. Lima-Neto, C.E.S. Nogueira, H.D.M. Coutinho, A.L.A.B. Leal, H.M. Barreto, N. Martins, Rodrigues Teixeira, A. M.;, H.S. Santos, Structural, Vibrational and Electrochemical Analysis and Antibacterial Potential of Isomeric Chalcones Derived from Natural Acetophenone, Applied Sciences, 10 (2020) 4713. http://dx.doi.org/10.3390/app10144713.

[20] T.S.d. Freitas, J.d.C. Xavier, R.L.S. Pereira, J.E. Rocha, D.F. Muniz, P.T. da Silva, J.P. da Hora, H.S. dos Santos, P.N. Bandeira, C.E.S. Nogueira, A.M.R. Teixeira, H.D.M. Coutinho, Direct antibacterial and antibiotic resistance modulatory activity of chalcones synthesized from the natural product 2-hydroxy-3,4,6-trimethoxyacetophenone, FEMS Microbiology Letters, 367 (2020). http://dx.doi.org/10.1093/femsle/fnaa124.

[21] C.A.N. Ferraz, S.R. Tintino, A.M.R. Teixeira, P.N. Bandeira, H.S. Santos, B.G. Cruz, C.E.S. Nogueira, T.F. Moura, R.L.S. Pereira, D.M. Sena, T.S. Freitas, J.E. Rocha, H.D.M. Coutinho, Potentiation of antibiotic activity by chalcone (E)-1-(4′-aminophenyl)-3-(furan-2-yl)-prop-2-en-1-one against gram-positive and gram-negative MDR strains, Microbial Pathogenesis, 148 (2020) 104453. https://doi.org/10.1016/j.micpath.2020.104453.

[22] P.T. da Silva, J.d.C. Xavier, T.S. Freitas, M.M. Oliveira, H.D.M. Coutinho, A.L.A.B. Leal, H.M. Barreto, P.N. Bandeira, C.E.S. Nogueira, D.M. Sena, F.W.Q. Almeida-Neto, E.S. Marinho, H.S. Santos, A.M.R. Teixeira, Synthesis, spectroscopic characterization and antibacterial evaluation by chalcones derived of acetophenone isolated from Croton anisodontus Müll.Arg, Journal of Molecular Structure, DOI https://doi.org/10.1016/j.molstruc.2020.129403(2021) 129403. https://doi.org/10.1016/j.molstruc.2020.129403.

[23] A.M.R. Teixeira, H.S. Santos, P.N. Bandeira, M.S.S. Juliao, P.T.C. Freire, V.N. Lima, B.G. Cruz, P.T. da Silva, H.D.M. Coutinho, D.M. Sena, Structural, spectroscopic and microbiological characterization of the chalcone 2E-1-(2 '-hydroxy-3 ',4 ',6 '-trimethoxyphenyl)-3-(phenyl)-prop-2-

en-1-one derived from the natural product 2-hydroxy-3,4,6-trimethoxyacetophenone, Journal of Molecular Structure, 1179 (2019) 739-748. https://doi.org/10.1016/j.molstruc.2018.11.075.

[24] P.N. Bandeira, R.O.S. Fontenelle, P.S. Costa, H.S. Santos, T.L.G. Lemos, Atividade Antifúngica In Vitro Contra Trychophyton Rubrum de P-Aminochalcones e 3'-Metoxi-4'-Hidroxi Chalcona, Revista Virtual de Química, 12 (2020) 703-711. https://doi.org/10.21577/1984-6835.20200056.

[25] Z. Rozmer, P. Perjési, Naturally occurring chalcones and their biological activities, Phytochemistry Reviews, 15 (2016) 87-120. https://doi.org/10.1007/s11101-014-9387-8.

[26] C.L. Zhuang, W. Zhang, C.Q. Sheng, W.N. Zhang, C.G. Xing, Z.Y. Miao, Chalcone: A Privileged Structure in Medicinal Chemistry, Chemical Reviews, 117 (2017) 7762-7810. http://dx.doi.org/10.1021/acs.chemrev.7b00020.

[27] P.N. Bandeira, T.L.G. Lemos, H. S. Santos, M.C.S. de Carvalho, D.P. Pinheiro, M.O. de Moraes Filho, C. Pessoa, F.W.A. Barros-Nepomuceno, T.H.S. Rodrigues, P.R.V. Ribeiro, H.S. Magalhães, A.M.R. Teixeira, Synthesis, structural characterization, and cytotoxic evaluation of chalcone derivatives, Medicinal Chemistry Research, DOI https://doi.org/10.1007/s00044-019-02434-1(2019). https://doi.org/10.1007/s00044-019-02434-1.

[28] T.R. Garcia, T.S. de Freitas, H.S. dos Santos, P.N. Bandeira, M.S.S. Julião, J.E. Rocha, C.E.S. Nogueira, R.L.S. Pereira, A.C.H. Barreto, P.T.C. Freire, H.D.M. Coutinho, A.M.R. Teixeira, Structural, vibrational and electrochemical analysis and antibiotic activity study of chalcone (2E)-1-(3′,-methoxy-4′,-hydroxyphenyl)-3-(3-nitrophenyl)prop-2-en-1-one, Journal of Molecular Structure, 1216 (2020) 128358. https://doi.org/10.1016/j.molstruc.2020.128358.

[29] T.O. Ajiboye, M.T. Yakubu, A.T. Oladiji, Electrophilic and Reactive Oxygen Species Detoxification Potentials of Chalcone Dimers is Mediated by Redox Transcription Factor Nrf-2, Journal of Biochemical and Molecular Toxicology, 28 (2014) 11-22. https://doi.org/10.1002/jbt.21517.

[30] M.K.A. Ferreira, A.W. da Silva, F.C.O. Silva, C.L.A. Holanda, S.M. Barroso, J.d.R. Lima, A.E. Vieira Neto, A.R. Campos, P.N. Bandeira, H.S. dos Santos, T.L.G. de Lemos, S.M.C. Siqueira, F.E.A. Magalhães, J.E.S.A. de Menezes, Anxiolytic-like effect of chalcone N-{(4′-[(E)-3-(4-fluorophenyl)-1-(phenyl) prop-2-en-1-one]} acetamide on adult zebrafish (Danio rerio): Involvement of the GABAergic system, Behavioural Brain Research, 374 (2019) 111871. https://doi.org/10.1016/j.bbr.2019.03.040.

[31] M.K.A. Ferreira, A.W. da Silva, F.C.O. Silva, A.E. Vieira Neto, A.R. Campos, S.A. Alves Rodrigues Santos, A.M. Rodrigues Teixeira, J. da Cunha Xavier, P.N. Bandeira, C.E. Sampaio Nogueira, D.H.A. de Brito, E.L. Rebouças, F.E.A. Magalhães, J. de Menezes, H.S. Dos Santos, Anxiolytic-like effect of chalcone N-{4'[(2E)-3-(3-nitrophenyl)-1-(phenyl)prop-2-en-1-one]} acetamide on adult zebrafish (Danio rerio): Involvement of the 5-HT system, Biochemical and Biophysical Research Communications, 526 (2020) 505-511. https://doi.org/10.1016/j.bbrc.2020.03.129.

[32] E.O. Ajaiyeoba, O.O. Ogbole, O.O. Abiodun, J.S. Ashidi, P.J. Houghton, C.W. Wright, Cajachalcone: An antimalarial compound from Cajanus cajan leaf extract, Journal of Parasitology Research 2013 (2013). https://doi.org/10.1155/2013/703781.

[33] X.W. Fang, B.Q. Yang, Z. Cheng, M.P. Yang, N. Su, L.Z. Zhou, J. Zhou, Synthesis and Antitumor Activity of Novel Nitrogen Mustard-Linked Chalcones, Archiv der Pharmazie, 346 (2013) 292-299. https://doi.org/10.1002/ardp.201200443.

[34] H. Wei, X. Zhang, G. Wu, X. Yang, S. Pan, Y. Wang, J. Ruan, Chalcone derivatives from the fern Cyclosorus parasiticus and their anti-proliferative activity, Food and Chemical Toxicology, 60 (2013) 147-152. https://doi.org/10.1016/j.fct.2013.07.045.

[35] C.E.S. Nogueira, M.M. de Oliveira, A.M.R. Teixeira, P.N. Bandeira, H.S. dos Santos, A.P. Ayala, B.P. Bezerra, A.C.H. Barreto, P.T.C. Freire, Crystal structure, FT-Raman and FTIR spectra and DFT calculations of chalcone (2E)-1-(4-aminophenyl)-3-(furan-2-yl)prop-2-en-1-one monohydrate, Journal of Molecular Structure, 1212 (2020) 128141. https://doi.org/10.1016/j.molstruc.2020.128141.

[36] A.D. Becke, Density-Functional Thermochemistry .1. The Effect of The Exchange-Only Gradient Correction, Journal of Chemical Physics, 96 (1992) 2155-2160. http://dx.doi.org/10.1063/1.462066.

[37] C. Lee, W. Yang, R.G. Parr, Development of the Colle-Salvetti correlation-energy formula into a functional of the electron density, Physical Review B, 37 (1988) 785-789. https://doi.org/10.1103/PhysRevB.37.785.

[38] J.d.C. Xavier, F.W.Q. Almeida-Neto, P.T. da Silva, E.S. Marinho, M.K.A. Ferreira, F.E.A. Magalhães, C.E.S. Nogueira, P.N. Bandeira, J.E.S.A. de Menezes, A.M.R. Teixeira, H.S.d. Santos, Structural characterization, electronic properties, and anxiolytic-like effect in adult zebrafish (Danio rerio) of cinnamaldehyde chalcone, Journal of Molecular Structure, 1222 (2020) 128954. https://doi.org/10.1016/j.molstruc.2020.128954.

[39] M.J. Frisch, G.W. Trucks, H.B. Schlegel, G.E. Scuseria, M.A. Robb, J.R. Cheeseman, G. Scalmani, V. Barone, B. Mennucci, G.A. Petersson, H. Nakatsuji, M. Caricato, X. Li, H.P. Hratchian, A.F. Izmaylov, J. Bloino, G. Zheng, J.L. Sonnenberg, M. Hada, M. Ehara, K. Toyota, R. Fukuda, J. Hasegawa, M. Ishida, T. Nakajima, Y. Honda, O. Kitao, H. Nakai, T. Vreven, J.A. Montgomery Jr., J.E. Peralta, F. Ogliaro, M.J. Bearpark, J. Heyd, E.N. Brothers, K.N. Kudin, V.N. Staroverov, R. Kobayashi, J. Normand, K. Raghavachari, A.P. Rendell, J.C. Burant, S.S. Iyengar, J. Tomasi, M. Cossi, N. Rega, N.J. Millam, M. Klene, J.E. Knox, J.B. Cross, V. Bakken, C. Adamo, J. Jaramillo, R. Gomperts, R.E. Stratmann, O. Yazyev, A.J. Austin, R. Cammi, C. Pomelli, J.W. Ochterski, R.L. Martin, K. Morokuma, V.G. Zakrzewski, G.A. Voth, P. Salvador, J.J. Dannenberg, S. Dapprich, A.D. Daniels, Ö. Farkas, J.B. Foresman, J.V. Ortiz, J. Cioslowski, D.J. Fox, Gaussian 09, Gaussian, Inc., Wallingford, CT, USA, 2009.

[40] R. Dennington, T. Keith, J. Millam, GaussView, Version 5, 2009.

[41] R. Cammi, J. Tomasi, Remarks on the use of the apparent surface charges (ASC) methods in solvation problems: Iterative versus matrix-inversion procedures and the renormalization of the apparent charges, Journal of Computational Chemistry, 16 (1995) 1449-1458. https://doi.org/10.1002/jcc.540161202.

[42] B. Mennucci, E. Cancès, J. Tomasi, Evaluation of Solvent Effects in Isotropic and Anisotropic Dielectrics and in Ionic Solutions with a Unified Integral Equation Method: Theoretical Bases, Computational Implementation, and Numerical Applications, The Journal of Physical Chemistry B, 101 (1997) 10506-10517. https://doi.org/10.1021/jp971959k.

[43] E. Cancès, B. Mennucci, J. Tomasi, A new integral equation formalism for the polarizable continuum model: Theoretical background and applications to isotropic and anisotropic dielectrics, The Journal of Chemical Physics, 107 (1997) 3032-3041. https://doi.org/10.1063/1.474659.

[44] S. Kaya, H. Gokce, T. Arslan, G. Alpaslan, Synthesis, spectroscopic characterization, DFT computations, nonlinear optical profile and molecular docking study of a novel chalcone derivative, Journal of Molecular Structure, 1202 (2020) 11. https://doi.org/10.1016/j.molstruc.2019.127270.

[45] M.H. Jamroz, Vibrational energy distribution analysis (VEDA): Scopes and limitations, Spectrochimica Acta Part a-Molecular and Biomolecular Spectroscopy, 114 (2013) 220-230. https://doi.org/10.1016/j.saa.2013.05.096.

[46] R. McWeeny, Perturbation Theory for the Fock-Dirac Density Matrix, Physical Review, 126 (1962) 1028-1034. http://dx.doi.org/10.1103/PhysRev.126.1028.

[47] R. Ditchfield, Self-consistent perturbation-theory of diamagnetism .1. Gauge-invariant LCAO method for NMR chemical-shifts, Molecular Physics, 27 (1974) 789-807. https://doi.org/10.1080/00268977400100711.

[48] K. Wolinski, J.F. Hinton, P. Pulay, Efficient implementation of the gauge-independent atomic orbital method for NMR chemical shift calculations, Journal of the American Chemical Society, 112 (1990) 8251-8260. http://dx.doi.org/10.1021/ja00179a005.

[49] R.G. Pearson, Hard and soft acids and bases, Journal of the American Chemical Society, 85 (1963) 3533-&. http://dx.doi.org/10.1021/ja00905a001.

[50] T. Koopmans, Über die Zuordnung von Wellenfunktionen und Eigenwerten zu den Einzelnen Elektronen Eines Atoms, Physica, 1 (1934) 104-113. https://doi.org/10.1016/S0031-8914(34)90011-2.

[51] H. Chermette, Chemical reactivity indexes in density functional theory, Journal of Computational Chemistry, 20 (1999) 129-154. http://dx.doi.org/10.1002/(SICI)1096-987X(19990115)20:1<129::AID-JCC13>3.0.CO;2-A.

[52] R.P. Iczkowski, J.L. Margrave, Electronegativity, Journal of the American Chemical Society, 83 (1961) 3547-3551. https://doi.org/10.1021/ja01478a001.

[53] R.G. Pearson, Recent advances in the concept of hard and soft acids and bases, Journal of Chemical Education, 64 (1987) 561. https://doi.org/10.1021/ed064p561.

[54] J.F. Janak, Proof that $\partial E/\partial ni = \epsilon i$ in density-functional theory, Physical Review B, 18 (1978) 7165-7168. https://doi.org/10.1103/PhysRevB.18.7165.

[55] L. Von Szentpály, Studies on electronegativity equalization: Part 1. Consistent diatomic partial charges, Journal of Molecular Structure: THEOCHEM, 233 (1991) 71-81. https://doi.org/10.1016/0166-1280(91)85055-C.

[56] W.T. Yang, R.G. Parr, Hardness, softness, and the Fukui function in the electronic theory of metals and catalysis, Proceedings of the National Academy of Sciences of the United States of America, 82 (1985) 6723-6726. https://doi.org/10.1073/pnas.82.20.6723.

[57] R.G. Parr, L.v. Szentpály, S. Liu, Electrophilicity Index, Journal of the American Chemical Society, 121 (1999) 1922-1924. https://doi.org/10.1021/ja983494x.

[58] P.K. Chattaraj, S. Giri, S. Duley, Update 2 of: Electrophilicity Index, Chemical Reviews, 111 (2011) PR43-PR75. https://doi.org/10.1021/cr100149p.

[59] Chemcraft - graphical software for visualization of quantum chemistry computations, 2006.

[60] K. Fukui, Role of frontier orbitals in chemical-reactions, Science, 218 (1982) 747-754. https://doi.org/10.1126/science.218.4574.747.

[61] I.B. Obot, D.D. Macdonald, Z.M. Gasem, Density functional theory (DFT) as a powerful tool for designing new organic corrosion inhibitors. Part 1: An overview, Corrosion Science, 99 (2015) 1-30. https://doi.org/10.1016/j.corsci.2015.01.037.

[62] C. Morell, A. Grand, A. Toro-Labbé, New Dual Descriptor for Chemical Reactivity, The Journal of Physical Chemistry A, 109 (2005) 205-212. https://doi.org/10.1021/jp046577a.

[63] J. Padmanabhan, R. Parthasarathi, M. Elango, V. Subramanian, B.S. Krishnamoorthy, S. Gutierrez-Oliva, A. Toro-Labbé, D.R. Roy, P.K. Chattaraj, Multiphilic Descriptor for Chemical Reactivity and Selectivity, The Journal of Physical Chemistry A, 111 (2007) 9130-9138. https://doi.org/10.1021/jp0718909.

[64] T. Lu, F. Chen, Multiwfn: A multifunctional wavefunction analyzer, Journal of Computational Chemistry, 33 (2012) 580-592. https://doi.org/10.1002/jcc.22885.

[65] K. Momma, F. Izumi, VESTA 3 for three-dimensional visualization of crystal, volumetric and morphology data, Journal of Applied Crystallography, 44 (2011) 1272-1276. https://doi.org/10.1107/s0021889811038970.

[66] A.-R. Allouche, Gabedit—A graphical user interface for computational chemistry softwares, Journal of Computational Chemistry, 32 (2011) 174-182. https://doi.org/10.1002/jcc.21600.

[67] F.L. Hirshfeld, Bonded-atom fragments for describing molecular charge densities, Theoretica Chimica Acta, 44 (1977) 129-138. https://doi.org/10.1007/BF00549096.

[68] N.M. O'Boyle, A.L. Tenderholt, K.M. Langner, cclib: A library for package-independent computational chemistry algorithms, Journal of Computational Chemistry, 29 (2008) 839-845. http://dx.doi.org/10.1002/jcc.20823.

[69] T. Yanai, D.P. Tew, N.C. Handy, A new hybrid exchange-correlation functional using the Coulomb-attenuating method (CAM-B3LYP), Chemical Physics Letters, 393 (2004) 51-57. https://doi.org/10.1016/j.cplett.2004.06.011.

[70] A.L. Alves Borges Leal, A.J.T. Machado, C.F. Bezerra, C.E. Serra Inácio, J.E. Rocha, D.L. Sales, T.S. de Freitas, W. de Oliveira Almeida, W.d. Amaral, L. Everson da Silva, A.P. Ferriani, B.H.L. de Noronha Sales Maia, M.F. Bezerra Morais-Braga, H.M. Barreto, H.D.M. Coutinho, Chemical identification and antimicrobial potential of essential oil of Piper rivinoides kunth (BETIS-WHITE), Food and Chemical Toxicology, 131 (2019) 110559. https://doi.org/10.1016/j.fct.2019.06.006.

[71] M.M. Oliveira, H.S. Santos, H.D.M. Coutinho, P.N. Bandeira, P.T. da Silva, T.S. Freitas, J.E. Rocha, J.C. Xavier, F.F. Campina, C.R.S. Barbosa, J.B. Araújo Neto, R.L.S. Pereira, M.M.C. Silva, D.F. Muniz, A.M.R. Teixeira, V.M. Frota, T.H.S. Rodrigues, A.M. Amado, M.P.M. Marques, L.A.E. Batista de Carvalho, C.E.S. Nogueira, Spectroscopic characterization and efflux pump modulation of a thiophene curcumin derivative, Journal of Molecular Structure, 1215 (2020) 128291. https://doi.org/10.1016/j.molstruc.2020.128291.

[72] A. Waterhouse, M. Bertoni, S. Bienert, G. Studer, G. Tauriello, R. Gumienny, F.T. Heer, T.A P. de Beer, C. Rempfer, L. Bordoli, R. Lepore, T. Schwede, SWISS-MODEL: homology modelling of protein structures and complexes, Nucleic Acids Research, 46 (2018) W296-W303. https://doi.org/10.1093/nar/gky427.

[73] O. Trott, A.J. Olson, AutoDock Vina: Improving the speed and accuracy of docking with a new scoring function, efficient optimization, and multithreading, Journal of Computational Chemistry, 31 (2010) 455-461. https://doi.org/10.1002/jcc.21334.

[74] Marvin Sketch, V. 20.15, Calculation Module Developed by ChemAxon, 2020.

[75] C.A. Lipinski, F. Lombardo, B.W. Dominy, P.J. Feeney, Experimental and computational approaches to estimate solubility and permeability in drug discovery and development settings, Advanced Drug Delivery Reviews, 23 (1997) 3-25. https://doi.org/10.1016/S0169-409X(96)00423-1.

[76] A. Daina, O. Michielin, V. Zoete, SwissADME: a free web tool to evaluate pharmacokinetics, drug-likeness and medicinal chemistry friendliness of small molecules, Scientific Reports, 7 (2017) 42717. https://doi.org/10.1038/srep42717.

[77] S. Yee, In Vitro Permeability Across Caco-2 Cells (Colonic) Can Predict In Vivo (Small Intestinal) Absorption in Man—Fact or Myth, Pharmaceutical Research, 14 (1997) 763-766. https://doi.org/10.1023/A:1012102522787.

[78] J. Kelder, P.D. Grootenhuis, D.M. Bayada, L.P. Delbressine, J.P. Ploemen, Polar molecular surface as a dominating determinant for oral absorption and brain penetration of drugs, Pharmaceutical Research, 16 (1999) 1514-1519. https://doi.org/10.1023/a:1015040217741.

[79] V. Prachayasittikul, P. Mandi, S. Prachayasittikul, V. Prachayasittikul, C. Nantasenamat, Exploring the Chemical Space of P-Glycoprotein Interacting Compounds, Mini Reviews in Medicinal Chemistry, 17 (2017) 1332-1345. https://doi.org/10.2174/1389557516666160121120344.

[80] B. Bienfait, P. Ertl, JSME: a free molecule editor in JavaScript, Journal of Cheminformatics, 5 (2013) 24. https://doi.org/10.1186/1758-2946-5-24.

[81] R.C. Braga, V.M. Alves, M.F. Silva, E. Muratov, D. Fourches, A. Tropsha, C.H. Andrade, Tuning HERG out: antitarget QSAR models for drug development, Current Topics in Medicinal Chemistry, 14 (2014) 1399-1415. https://doi.org/10.2174/1568026614666140506124442.

[82] B.E. KSOZ, R. ERTAN, Chemical and Structural Properties of Chalcones I, FABAD Journal of Pharmaceutical Sciences, 36 (2011) 232-242.

[83] I.K.C. Lima, F.D. de Sousa, A.J.d.M. Bento, B.G. Cruz, P.T. da Silva, P.N. Bandeira, H.S. dos Santos, G.D. Saraiva, A.C.H. Barreto, P.d.T.C. Freire, A.M.R. Teixeira, Structural and spectroscopic investigation of the chalcones (E)-1-(4-aminophenyl)-3-(4′-ethoxyphenyl)-prop-2-en-

1-one and (E)-1-(aminophenyl)-3-(4′-methoxyphenyl)-prop-2-en-1-one, Vibrational Spectroscopy, 110 (2020) 103118. https://doi.org/10.1016/j.vibspec.2020.103118.

[84] C. Parlak, P. Ramasami, Theoretical and experimental study of infrared spectral data of 2-bromo-4-chlorobenzaldehyde, SN Applied Sciences, 2 (2020) 1148. http://dx.doi.org/10.1007/s42452-020-2935-5.

[85] E. Echegaray, C. Cárdenas, S. Rabi, N. Rabi, S. Lee, F.H. Zadeh, A. Toro-Labbe, J.S.M. Anderson, P.W. Ayers, In pursuit of negative Fukui functions: examples where the highest occupied molecular orbital fails to dominate the chemical reactivity, Journal of Molecular Modeling, 19 (2013) 2779-2783. https://doi.org/10.1007/s00894-012-1637-3.

[86] E. Echegaray, S. Rabi, C. Cárdenas, F.H. Zadeh, N. Rabi, S. Lee, J.S.M. Anderson, A. Toro-Labbe, P.W. Ayers, In pursuit of negative Fukui functions: molecules with very small band gaps, Journal of Molecular Modeling, 20 (2014) 2162. https://doi.org/10.1007/s00894-014-2162-3.

[87] U.M. Hanumegowda, G. Wenke, A. Regueiro-Ren, R. Yordanova, J.P. Corradi, S.P. Adams, Phospholipidosis as a Function of Basicity, Lipophilicity, and Volume of Distribution of Compounds, Chemical Research in Toxicology, 23 (2010) 749-755. https://doi.org/10.1021/tx9003825.

[88] P. Ertl, B. Rohde, P. Selzer, Fast Calculation of Molecular Polar Surface Area as a Sum of Fragment-Based Contributions and Its Application to the Prediction of Drug Transport Properties, Journal of Medicinal Chemistry, 43 (2000) 3714-3717. https://doi.org/10.1021/jm000942e.

[89] D.F. Veber, S.R. Johnson, H.Y. Cheng, B.R. Smith, K.W. Ward, K.D. Kopple, Molecular properties that influence the oral bioavailability of drug candidates, Journal of Medicinal Chemistry, 45 (2002) 2615-2623. https://doi.org/10.1021/jm020017n.

[90] T. Fichert, M. Yazdanian, J.R. Proudfoot, A structure–Permeability study of small drug-like molecules, Bioorganic & Medicinal Chemistry Letters, 13 (2003) 719-722. https://doi.org/10.1016/S0960-894X(02)01035-1.

[91] W.M. Pardridge, Blood-brain barrier genomics and the use of endogenous transporters to cause drug penetration into the brain, Current opinion in drug discovery & development, 6 (2003) 683-691.

[92] M. Olivo, R. Bhuvaneswari, S.S. Lucky, N. Dendukuri, P. Soo-Ping Thong, Targeted Therapy of Cancer Using Photodynamic Therapy in Combination with Multi-faceted Anti-Tumor Modalities, Pharmaceuticals (Basel, Switzerland), 3 (2010) 1507-1529. https://doi.org/10.3390/ph3051507.

[93] D. D'Eliseo, F. Velotti, Omega-3 Fatty Acids and Cancer Cell Cytotoxicity: Implications for Multi-Targeted Cancer Therapy, Journal of Clinical Medicine, 5 (2016). https://doi.org/10.3390/jcm5020015.

[94] N. Takebe, P.J. Harris, R.Q. Warren, S.P. Ivy, Targeting cancer stem cells by inhibiting Wnt, Notch, and Hedgehog pathways, Nature Reviews: Clinical Oncology, 8 (2011) 97-106. https://doi.org/10.1038/nrclinonc.2010.196.

[95] B.N. Ames, K. Hooper, Does carcinogenic potency correlate with mutagenic potency in the Ames assay?, Nature, 274 (1978) 19-20. https://doi.org/10.1038/274019a0.

[96] J.M. Kratz, U. Grienke, O. Scheel, S.A. Mann, J.M. Rollinger, Natural products modulating the hERG channel: heartaches and hope, Natural Products Reports, 34 (2017) 957-980. https://doi.org/10.1039/c7np00014f.

[97] N. Chiesa, B. Rosati, A. Arcangeli, M. Olivotto, E. Wanke, A novel role for HERG K+ channels: spike-frequency adaptation, Journal of Physiology, 501 (Pt 2) (1997) 313-318. https://doi.org/10.1111/j.1469-7793.1997.313bn.x.

[98] J.L. Overholt, E. Ficker, T. Yang, H. Shams, G.R. Bright, N.R. Prabhakar, HERG-Like potassium current regulates the resting membrane potential in glomus cells of the rabbit carotid body, Journal of Neurophysiology, 83 (2000) 1150-1157. https://doi.org/10.1152/jn.2000.83.3.1150.

[99] M.C. Sanguinetti, M. Tristani-Firouzi, hERG potassium channels and cardiac arrhythmia, Nature, 440 (2006) 463-469. https://doi.org/10.1038/nature04710.

[100] A. Arcangeli, Expression and role of hERG channels in cancer cells, Novartis Foundation Symposium, 266 (2005) 225-232; discussion 232-224.

[101] B. Meunier, S.P. de Visser, S. Shaik, Mechanism of Oxidation Reactions Catalyzed by Cytochrome P450 Enzymes, Chemical Reviews, 104 (2004) 3947-3980. https://doi.org/10.1021/cr020443g.

[102] D. Korolev, K.V. Balakin, Y. Nikolsky, E. Kirillov, Y.A. Ivanenkov, N.P. Savchuk, A.A. Ivashchenko, T. Nikolskaya, Modeling of Human Cytochrome P450-Mediated Drug Metabolism Using Unsupervised Machine Learning Approach, Journal of Medicinal Chemistry, 46 (2003) 3631-3643. https://doi.org/10.1021/jm030102a.

[103] L.M. Rezende-Junior, L.M. de Sousa Andrade, A.L. Alves Borges Leal, A.B. de Souza Mesquita, A.L. Portela de Araujo dos Santos, J.d.S. Lima Neto, J.P. Siqueira-Junior, C.E. Sampaio Nogueira, G.W. Kaatz, H.D. Melo Coutinho, N. Martins, C.Q. Rocha, H.M. Barreto, Chalcones Isolated fromArrabidaea brachypodaFlowers as Inhibitors of NorA and MepA Multidrug Efflux Pumps of Staphylococcus aureus, Antibiotics-Basel, 9 (2020). https://doi.org/10.3390/antibiotics9060351.

Fig. 1. Optimized geometry of the title chalcone obtained at B3LYP/6-311++G(d,p) level of theory.

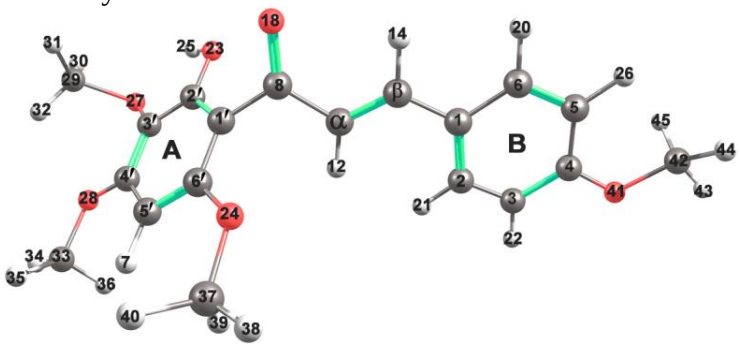

Fig 2. (a) Potential energy profiles of the title chalcone calculated at the B3LYP/6-311++G(d,p) level of theory for rotation around C6-C1-Cβ-Cα dihedral angle. The global and local minima for the optimized structures are indicated by means of open circle, and half open circle. In (b) and (c) are shown the conformers I and II, respectively, with their respective dihedral angle (θ), and potential energies (E), and with the blue planes containing the A ring, and the red planes containing the B ring.

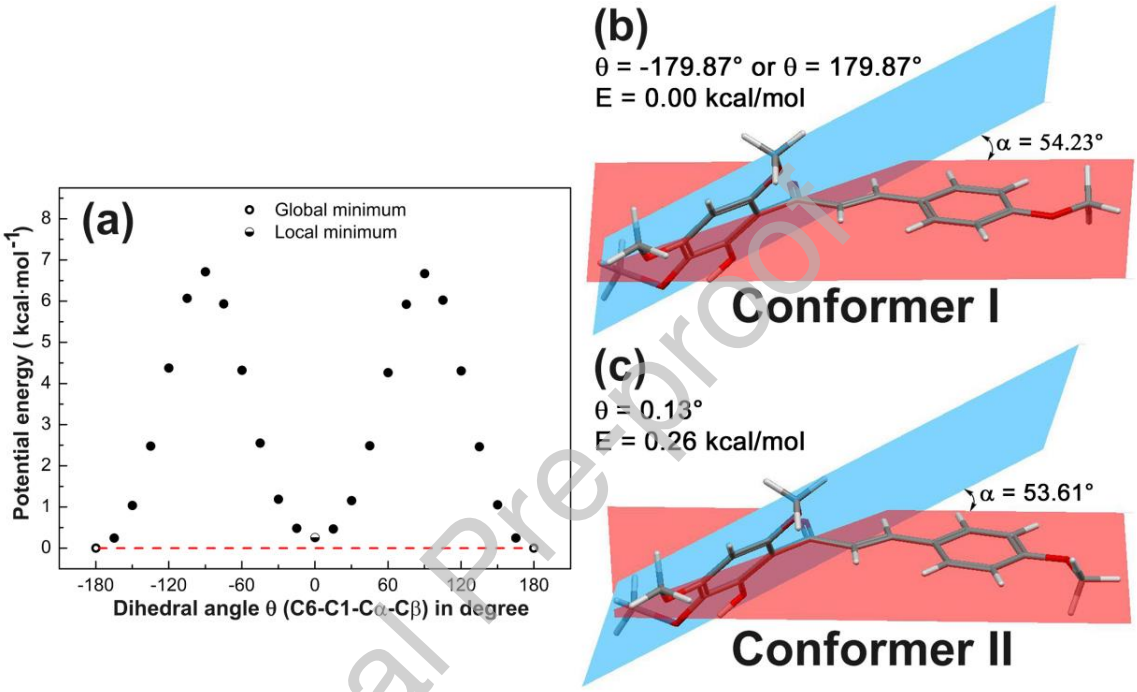

Fig. 3. Experimental ATR-IR and theoretical Infrared spectrum obtained at B3LYP/6-311++G(d,p) level of theory.

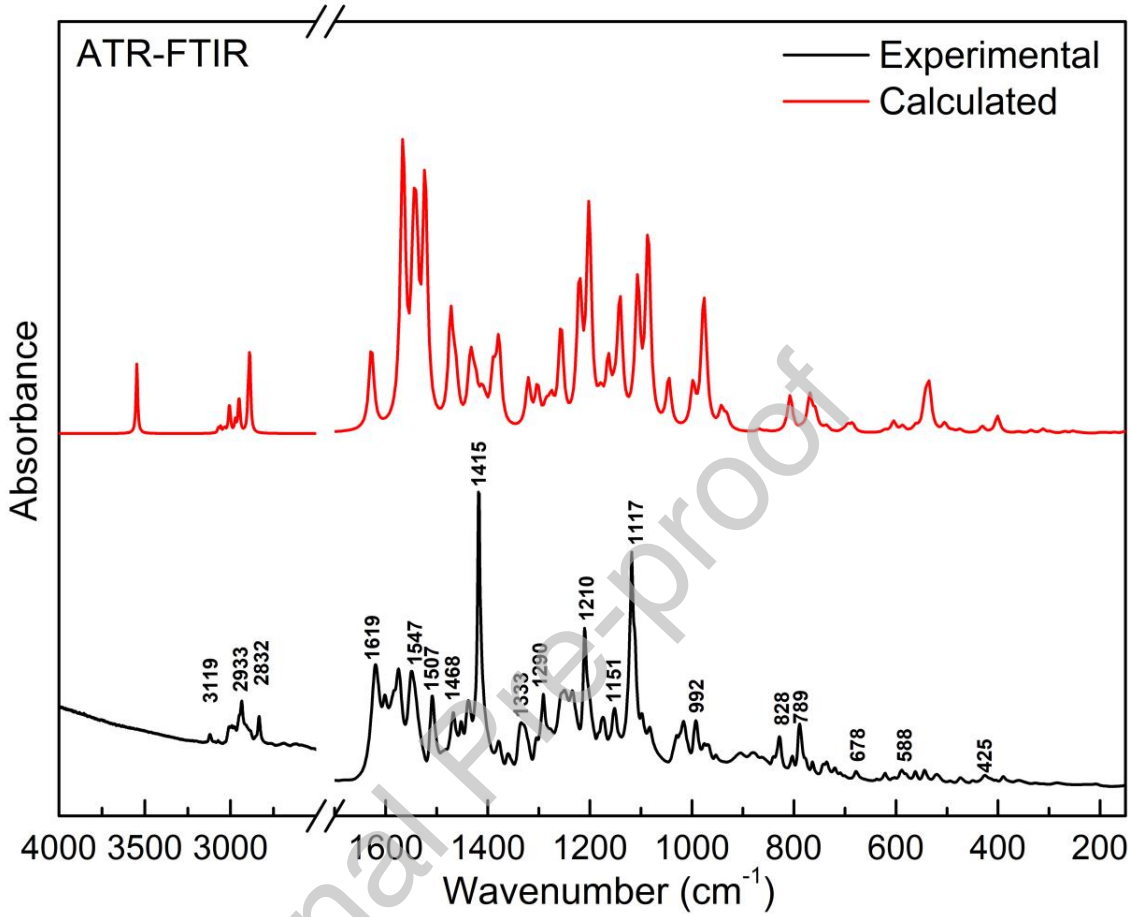

Fig. 4. Frontier Molecular Orbitals (HOMO and LUMO) calculated for title chalcone at B3LYP/6-311++G(d,p) level of theory.

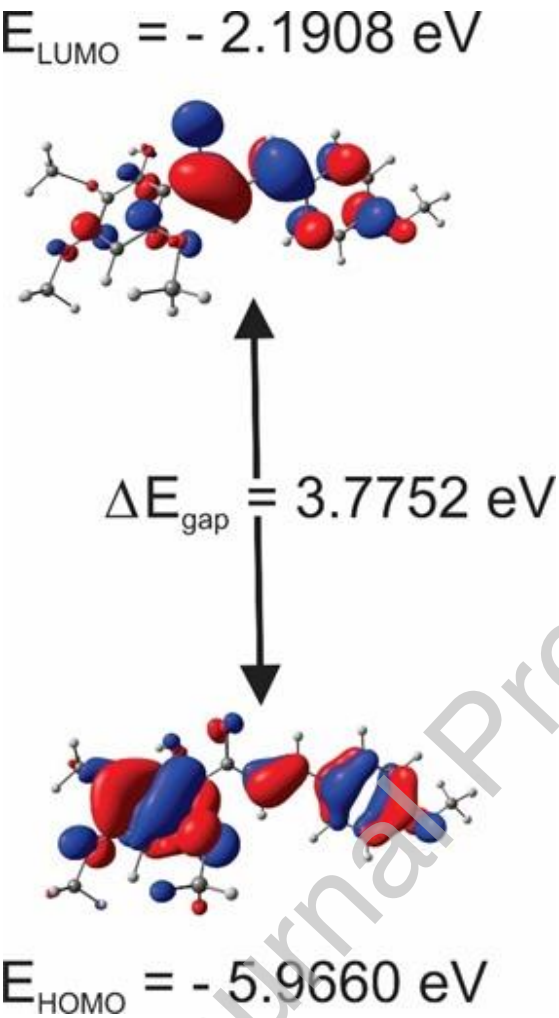

Fig. 5. The Electronic Fukui functions for the nucleophilic attack (f^+), electrophilic attack (f^-), and radical attack (f^0) obtained with isodensity value 0.00072736 of the title chalcone.

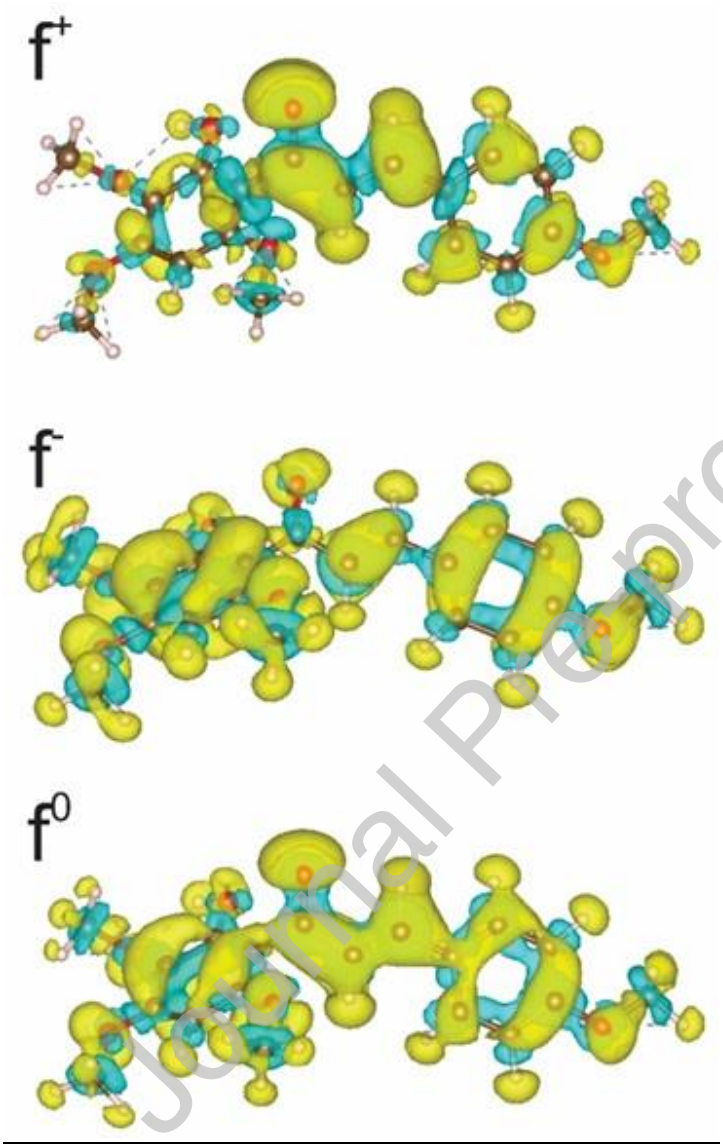

Fig. 6. Calculated Molecular Electrostatic Potential (MEP) for title chalcone at B3LYP/6-311++G(d,p) level of theory.

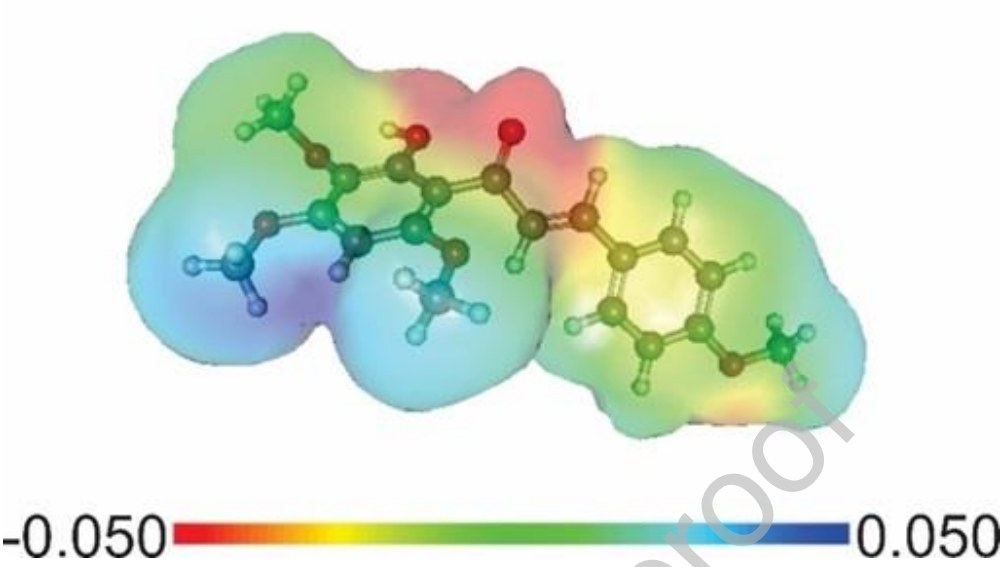

Fig. 7. Experimental UV–Vis spectrum of the title chalcone

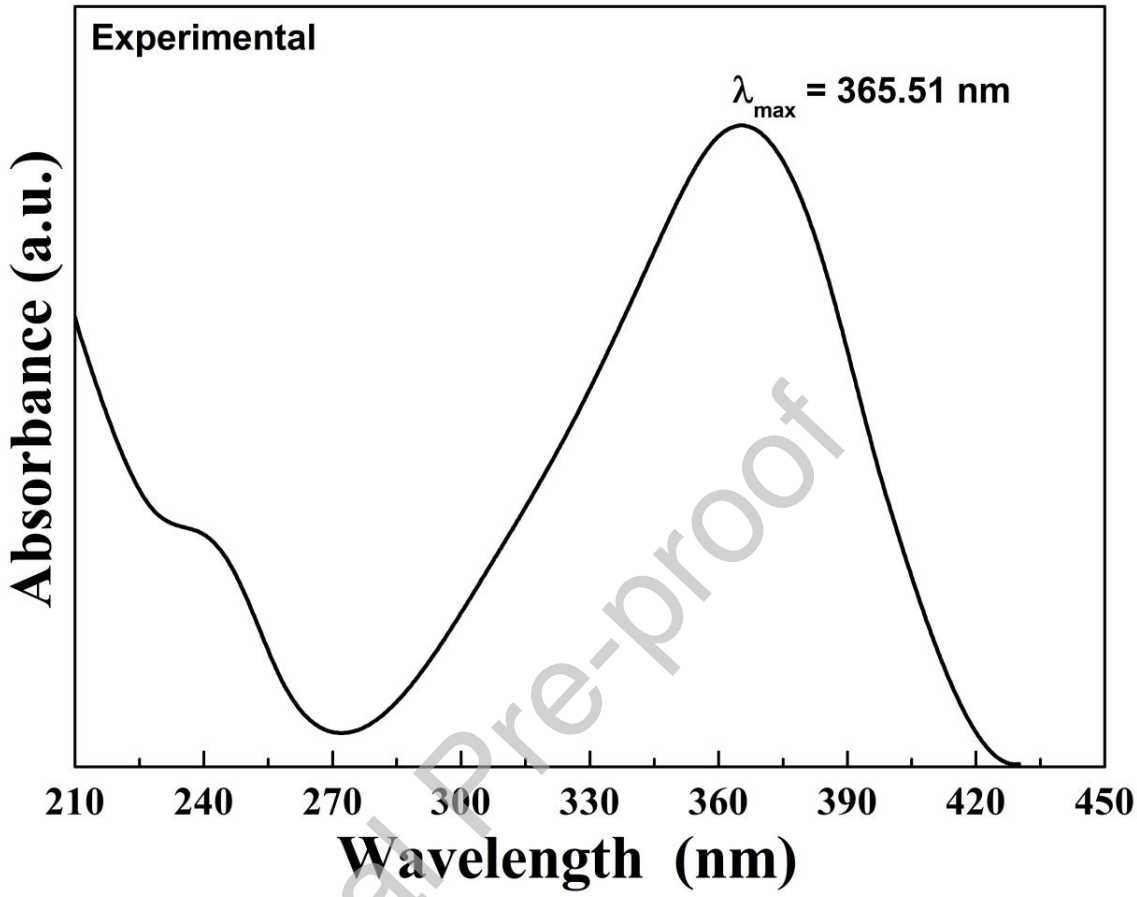

Fig. 8. Theoretical UV–Vis spectrum of the title chalcone using the TD-DFT method with the CAM-B3LYP/6-311++G(d,p) level of theory and ethanol as an implicit solvent.

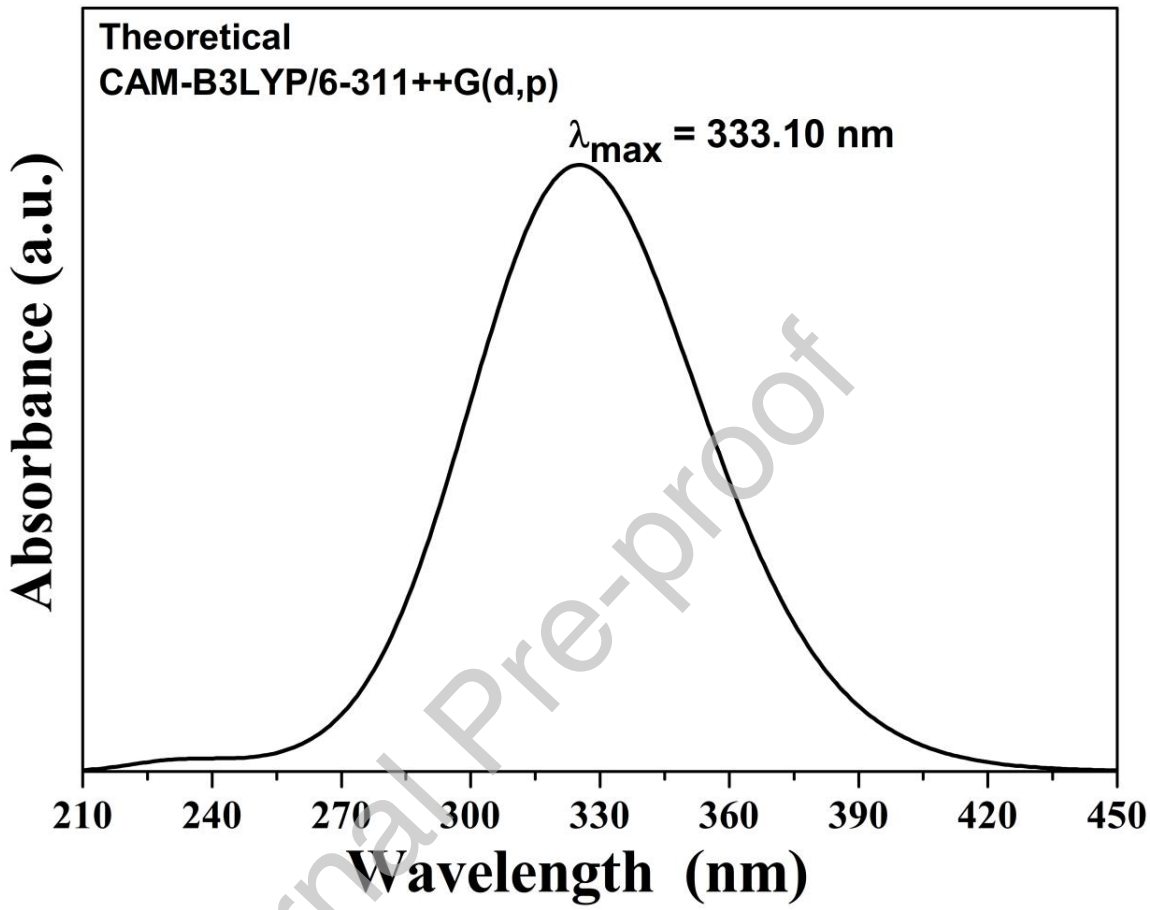

Fig. 9. Graph of the distribution of chalcone micro species as a function of pH variation through the acid dissosiation constant (pKa).

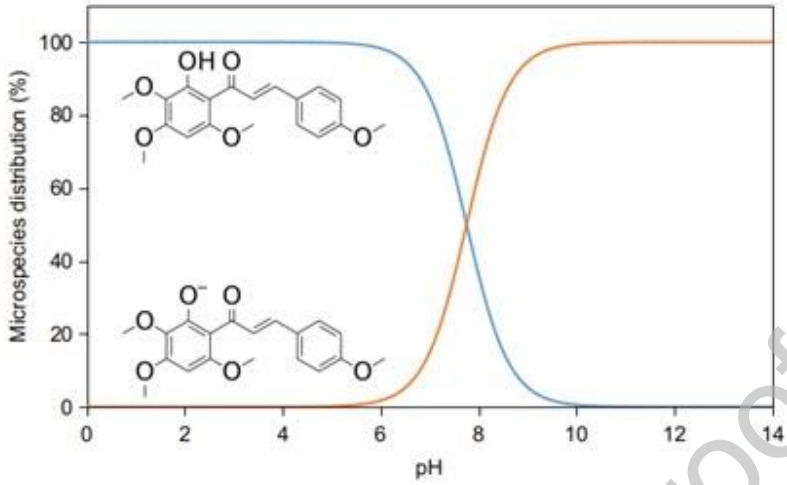

Fig. 10. Bioavailability radar of the title chalcone L by the druglikeness criteria (Lipophilicity (-0.7 < log P < 5.0), size (150 g/mol < MW < 500 g/mol), polarity (20Å² < TPSA < 130 Å²), insolubility (-6 < log S < 0), insaturação (0.25 < Fraction Csp3 < 1) and flexibility (0 < Num. Rotatable bonds < 9).

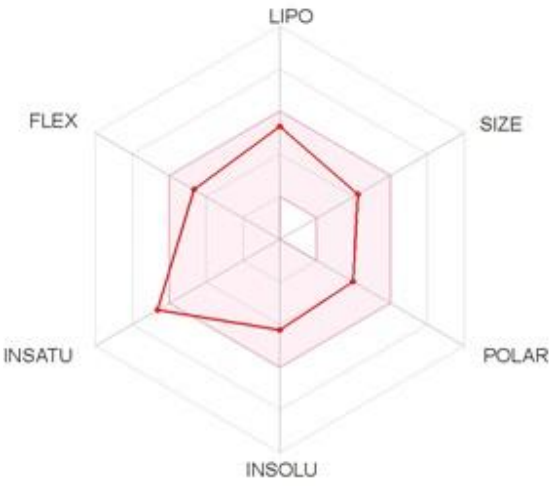

Fig. 11. Models of structure-activity relationship (QSAR) of chalcone: A - absorption represented by the log D and pH values, B - solubility class represented by the log S and pH values, C - water solubility represented by the concentration in mg/mL and pH values and D - Molecular fragments of the acute oral toxicity model.

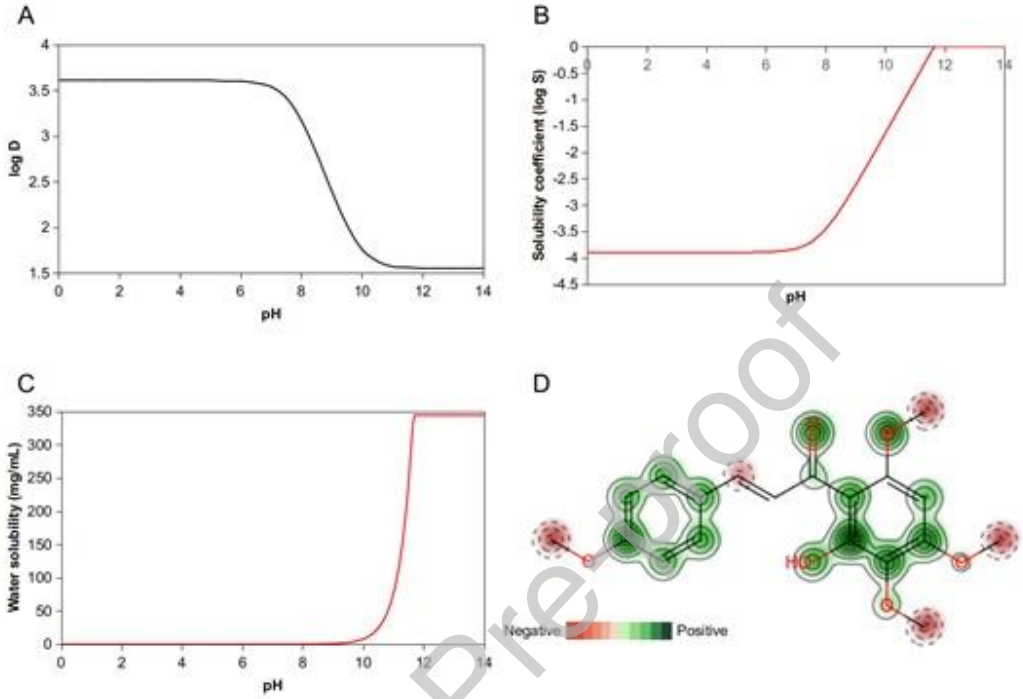

Fig. 12. MICs of the Ciprofloxacin (Cip) and Ethidium Bromide (EB) in the absence or presence of binary mixture acetophenone (59.14%) and title chalcone (40.86 %), as well as Chlorpromazine (CPZ) and carbonylcyanide m-chlorophenyl hydrazone (CCCP) against K2068 (MepA).

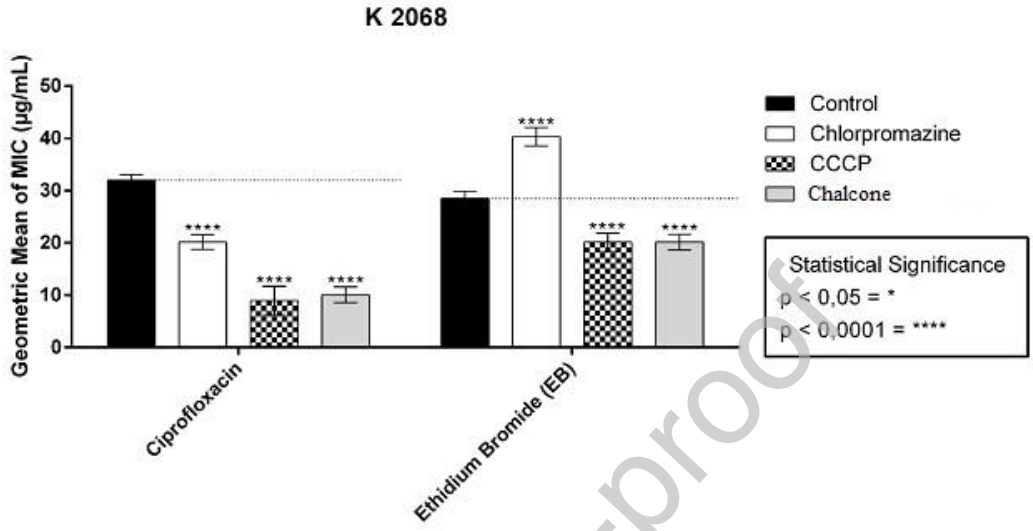

Fig. 13. The best pose of chalcone (pink) and the best pose of ciprofloxacin (blue) on the binding site of the MepA model.

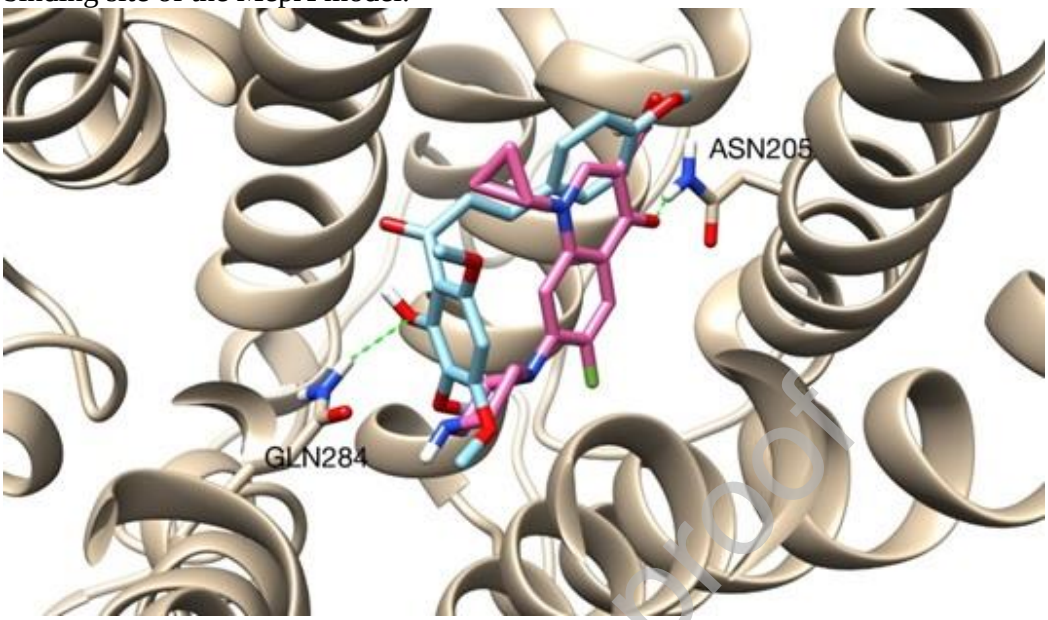

Fig. 14. 2D ligand-protein interaction diagram of the title chalcone and the MepA model. Contact distances are shown in green.

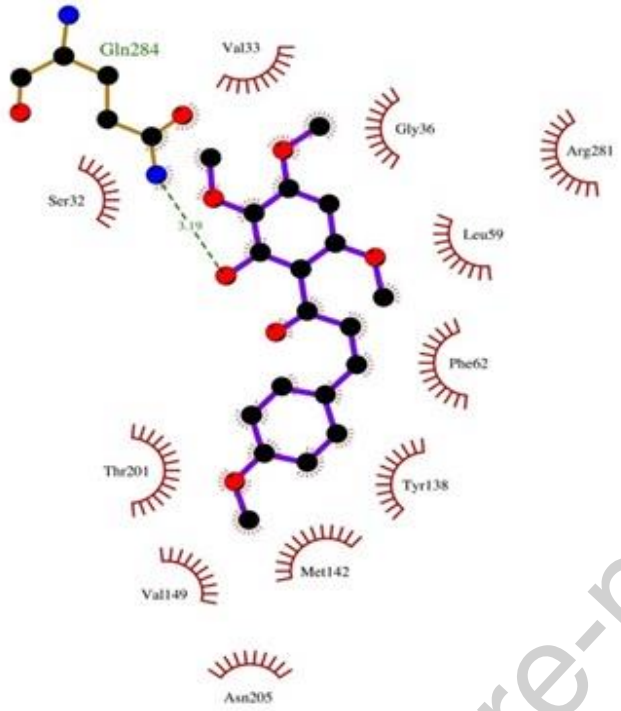

Scheme 1. Preparation of chalcone. a) NaOH 50 % w v^{-1}, ethanol, t.a., 48 h.

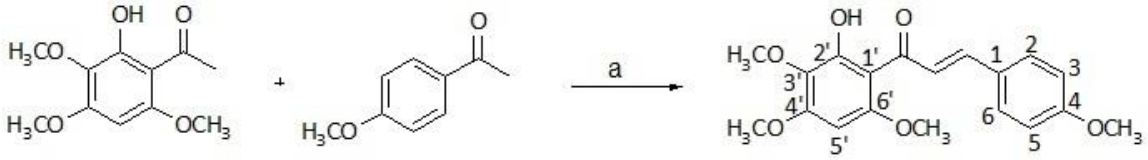

Table 1. ^{1}H and ^{13}C NMR data of the experimental and theoretical of title clalcone in $CDCl_3$. Chemical shifts in δ_C and δ_H are in ppm.

Chalcone				
C	δ_C	δ_H	δc (calc)	δ_H (calc)
1'	107.1		119.62645	
2'	158.7		158.73965	
3'	130.3		136.06635	
4'	159.5		162.63845	
5'	87.3	5.93 (s)	89.05915	5.9333417
6'	158.6		163.82965	
MeO	60.9	3.78 (s)	57.79455	3.7992417
MeO	56.2	3.86 (s)	57.34895	3.7871417
MeO	55.8	3.90 (s)	57.44635	3.8286417
MeO	55.5	3.91 (s)	62.94755	3.8801417
C=O	193.3		198.28065	
1	130.7		134.79935	
2/6	125.2	7.53 (d, *J* = 8.4 Hz)	133.55165	7.7428417
3/5	130.3	7.89 (d, *J* = 8.4 Hz)	143.30375	7.2150417
4	131.0		124.87655	
C_α	128.4	7.24 (d, *J* = 14.6 Hz)	114.79385	7.3393417
C_β	142.9	7.75 (d, *J* = 14.6 Hz)	171.32305	8.0473417

Table 2. ATR-FTIR experimental frequencies ($\tilde{\nu}_{\text{ATR-FTIR}}$, in cm^{-1}), calculated scaled vibrational wavenumbers ($\tilde{\nu}_{\text{scal}}$ in cm^{-1}) by the dual scale factor 0.983 (below 1700 cm^{-1}) and 0.958 (above 1700 cm^{-1}) and assignment for some of the vibrational modes for title chalcone ($C_{19}H_{20}O_6$) associated with the bands of the infrared absorbance spectrum show in Figure 4.

EXP $\tilde{\nu}_{\text{ATR-FTIR}}$ (cm^{-1})	DFT $\tilde{\nu}_{\text{scal}}$ (cm^{-1})	Assignment for some absorbance bands for title chalcone ($C_{19}H_{20}O_6$)
3119	3012.795	ν (CβH14) (97)
2933	2950.918	υ_{as}(C37H39) (48) + υ_{as}(C37H40) (51)
2832	2889.462	υ_{s}(C37H40) (44) + υ_{s}(C37H39) (46)
1619	1629.596	ν (CαCβ) (24) + ν (C8O18) (17)
1547	1564.356	ν (CαCβ) (12) + ν (C4C5) (21)
1507	1512.355	β (H21C2C3) (14) + β (H20C6C5) (14) + β (H22C3C4) (14) + β (H26C5C6) (15)
1468	1462.183	β (H39C37H38) (16) + β (H34C33H36) (22) + β (H35C33H34) (29) + β (H38C37H40) (30)

1415	1415.884	ν (C3′C2′) (16) + ν (C2′C1′) (16) + ν (O23C2′) (18)
1333	1318.36	β (H21C2C3) (10) + β (H12Cα Cβ) (11) + ν (CβCα) (11) + β (H14CβCα) (15)
1290	1290.679	β (H21C2C3) (11) + ν (CβC1′) (14) + β (H14CβCα) (18)
1210	1234.353	β (H7C5′C4′) (14) + ν (O27C3′) (26)
1151	1136.358	ν (O28C33) (11) + ν (O28C4′) (17)
1117	1114.958	ν (O24C37) (16) + ν (O23C2′) (20)
992	1002.139	β (C4C5C6) (12) + β (C2C3C4) (21) + ν (O27C29) (23)
828	829.4751	γ (O41C3C5C4) (10) + τ (H22C3C4C5) (10) + τ (H21C2C3C4) (13)
678	703.887	γ (O28C5′C3′C4′) (13) + γ (O24C5′C1′C6′) (14)
588	557.7345	τ (H25O23C2′C3′) (82)
425	411.6313	β (C33O28C4′) (13) + β (C6C1Cβ) (15)

Nomenclature: τ =torsion; γ = deformation out of plane; δ = deformation; ν = stretching; ν_{as} = asymmetric stretching; ν_s = symmetric stretching.

Table 3. Calculated quantum reactivity descriptors for title chalcone computed at B3LYP/6-311++G(d,p) level of theory.

Quantum reactivity descriptor	Chalcone (In this work)	PAAPFBA (Ref. [17])	Cinnamaldehyde (Ref. [38])
HOMO energy (E_{HOMO}/ eV)	-5.96603	-6.58330	-6.06057
LUMO energy (E_{LUMO}/ eV)	-2.19084	-2.68007	-2.69721
Energy Gap (ΔE_{GAP}/ eV)	3.775189	3.903232	3.363354
Ionization Potential (I / eV)	5.966034	6.583302	6.060568
Electron Affinity (A / eV)	2.190845	2.68007	2.697214
Electronegativity (χ / eV)	4.078439	4.631686	4.378891
Global Hardness (η / eV)	1.887595	1.951616	1.681677
Global Softness (S / eV^{-1})	0.529775	0.512396	0.594645
Electrophilicity Index (ω / eV)	4.406049	5.496091	5.701061
Nucleophilicity Index (ε / eV^{-1})	0.226961	0.181947	0.175406

Table 4. Condensed Fukui functions, the dual descriptor (Δf), and the multiphilic index (Δω) calculated from the Hirshfeld charge analysis for the anionic, neutral, and cationic species of the title chalcone.

Atom	f^+	f^-	f^0	Δf	Δω
C3'	-0.01171	-0.05893	-0.03532	0.047228	0.208089
C4'	-0.02256	-0.0352	-0.02888	0.012637	0.055679
C2'	-0.01691	-0.01906	-0.01798	0.002149	0.009469
C1'	-0.00571	-0.04048	-0.02309	0.034768	0.15319
C6'	-0.01533	-0.03728	-0.02631	0.021951	0.096717

C5'	-0.01372	-0.02216	-0.01794	0.008435	0.037165
H7	-0.00959	-0.01433	-0.01196	0.004739	0.02088
C8	-0.09686	-0.01172	-0.05429	-0.08514	-0.37515
Cα	-0.0644	-0.04803	-0.05621	-0.01638	-0.07215
O18	-0.118	-0.03586	-0.07693	-0.08214	-0.3619
Cβ	-0.10464	-0.03139	-0.06801	-0.07325	-0.32276
H12	-0.03088	-0.01429	-0.02258	-0.01659	-0.07311
C1	-0.02126	-0.03813	-0.0297	0.016873	0.074343
H14	-0.04153	-0.01647	-0.029	-0.02506	-0.11041
C2	-0.03923	-0.02333	-0.03128	-0.0159	-0.07004
C6	-0.04183	-0.03197	-0.0369	-0.00986	-0.04344
C3	-0.02646	-0.03012	-0.02829	0.003664	0.016144
C5	-0.02567	-0.03105	-0.02836	0.005373	0.023674
C4	-0.04719	-0.03945	-0.04332	-0.00774	-0.03412
H20	-0.02091	-0.01694	-0.01893	-0.00398	-0.01752
H21	-0.0201	-0.0124	-0.01625	-0.00771	-0.03395
H22	-0.01822	-0.01705	-0.01764	-0.00118	-0.00518
H23	-0.0106	-0.02066	-0.01563	0.010062	0.044334
O24	-0.00508	-0.04054	-0.02281	0.035455	0.156216
H25	-0.00997	-0.01183	-0.0109	0.001851	0.008156
H26	-0.01631	-0.01629	-0.0163	-1.7E-05	-7.5E-05
O27	-0.0065	-0.02923	-0.01786	0.022737	0.10018
O28	-0.01272	-0.03242	-0.02257	0.019705	0.086821
C29	-0.0045	-0.01307	-0.00878	0.008572	0.037769
H30	-0.00529	-0.01215	-0.00872	0.006858	0.030217
H31	-0.003	-0.01044	-0.00672	0.007445	0.032803
H32	-0.00383	-0.00845	-0.00614	0.004617	0.020343
C33	-0.00546	-0.0115	-0.00848	0.006042	0.026621
H34	-0.00609	-0.01078	-0.00844	0.004689	0.02066
H35	-0.00481	-0.01043	-0.00762	0.005614	0.024736
H36	-0.00457	-0.01011	-0.00734	0.005534	0.024383
C37	-0.00699	-0.01325	-0.01012	0.006255	0.02756
H38	-0.00554	-0.01103	-0.00829	0.005494	0.024207
H39	-0.00631	-0.01248	-0.0094	0.006171	0.02719
H40	-0.00823	-0.01425	-0.01124	0.006018	0.026516
O41	-0.02538	-0.04163	-0.0335	0.016248	0.071589
C42	-0.00946	-0.01156	-0.01051	0.002094	0.009226
H43	-0.00939	-0.01035	-0.00987	0.00096	0.00423
H44	-0.00841	-0.0109	-0.00966	0.002487	0.010958
H45	-0.00839	-0.01093	-0.00966	0.002533	0.011161

Table 5. Physicochemical and pharmacokinetics properties by the ADMET parameters for title chalcone

Physicochemical		ADMET	
Properties	Value	Properties	Value

MW	344.36 g/mol	Absorption	HIA	High
Clog P	3.61		Caco-2	Moderately
log $D_{pH7.4}$	3.45	Distribution	BBB	No
log $S_{pH7.4}$	-3.74		Pgp	Yes
Wsol	0.06	Metabolism	GPCR	-0.10
HBD	1		Ion CM	-0.08
HBA	6		Kinase	-0.18
TPSA	74.22 Å²		Nuclear	-0.03
Nrot	7		Protease	-0.20
Fsp3	0.21		Enzyme	0.02
Nvio	0	Toxicity	Acute oral	Non-toxic

legend: MW (molecular weight (g/mol)), Clog P (consensus partition coefficient), log $D_{pH7.4}$ (distribution coefficient at pH 7.4), log $S_{pH7.4}$ (solubility coefficient at pH 7.4), Wsol (water solubility (mg/mL)), HBD (hydrogen bond donor count), HBA (hydrogen bond acceptor count), TPSA (topological polar surface area (Å²)), Nrot (number of rotatable bonds), Fsp3 (fraction Csp3), Nvio (number of violations by the Lipinski and Veber druglikeness criteria), HIA (human intestinal absorption), Caco-2 (human adenocarcinoma colon cells), BBB (blood-brain barrier penetration), Pgp (P-glycoprotein substrate), bioactivity by the GPCR (G-protein coupled receptor), ion CM (ion channel modulator), kinase inhibitor, nuclear receptor ligand, protease inhibitor and enzyme inhibitor models and toxicity by the acute oral model.